FINAL REPORT

U.S. Department of Energy

COLLABORATIVE RESEARCH: HYDROGEOLOGICAL-GEOPHYSICAL METHODS FOR SUBSURFACE SITE CHARACTERIZATION

Principal Investigator: Gary Mavko

Stanford University

Project No: 54655

Contract Number: DE-FG07-96ER 14723

Contract Project Officer: **Jose L. Elizondo and Thomas W. Hillebrant**

Project Duration: 09/15/96 – 12/31/99.

TABLE OF CONTENTS

EXECUTIVE SUMMARY

The objective of this research has been to improve aquifer characterization. This objective was met by focusing on using rock physics theory and geophysical data to predict flow properties, such as porosity, permeability and clay content. The advantage of using geophysical data to predict these properties stems from the fact that geophysical data are less expensive and more spatially-abundant than lab- or field-measured, flow-property data. This research contributes three newly-developed relationships that significantly improve aquifer characterization: (1) a general relationship between total and channel porosities, (2) a general relationship between electrical resistivity and channel porosity, and (3) bounds on the electrical resistivity – seismic velocity relationship.

The objective of aquifer characterization is to create hydrogeologic maps of the geometries of aquifers and aquitards and their flow properties, such as porosity and permeability. Without characteristic hydrogeologic maps, hydraulic flow and contaminant transport cannot be accurately modeled. Historically, hydrogeologic maps have been created by *qualitatively* interpolating flow properties between wells using hydraulic, chemistry and lithologic well data. However, over the past few decades, geostatistical techniques and geophysical data have been used in addition to traditional data analysis techniques to *quantitatively* interpolate flow properties throughout the well columns and away from wells where data do not exist. These innovative techniques have proven to be more cost-efficient and less subjective than traditional ones.

The research in this project was focused on developing better techniques for characterizing aquifer environments, a much-needed area of research. The first part of the work focuses on basic data exploration from a field site chosen for the collaborative part of the study. We were able to find correlations between geophysical observations and sediment types. We were also able to conclude from a rigorous analysis of bounds that certain low seismic velocity anomalies could only be explained by undersaturation. This portion of the study also highlighted the need for improved rock physics relations among porosity, permeability, electrical resistivity and seismic velocities.

The second part of the work includes new developments for constraining porosity estimates. In particular, it focuses on developing the relationship between channel and total porosities and discussing how porosity is defined physically, hydraulically, electrically and seismically. Channel porosity is the fraction of the total pore volume fraction of a composite that is available for hydraulic and electrical flow. The total porosity is the total pore volume fraction of a composite; a controlling factor for the response of seismic waves. We show that a composite's channel porosity can be related to its total porosity by its porous percolation threshold, critical porosity, and a pore space parameter. The percolation threshold and critical porosity define three distinct porosity regions physically, hydraulically, electrically and seismically. Region I is defined for porosities less than the porous percolation threshold, Region II is defined for porosities between the porous percolation threshold and critical porosity, and Region III is defined for porosities greater than the critical porosity. The channel porosity – total porosity relationship is valuable for converting from channel to total porosity or vise versa when (1) comparing lab-measured and estimated porosities with hydraulic permeability,

formation resistivity factor, or seismic velocity data, and (2) relating seismic velocity data to resistivity or permeability data. The most significant contributions of this work are (1) the development of the total porosity – channel porosity relationship, and (2) insight into the relationships between channel porosity and formation factor and between channel porosity and permeability.

The next part of the project focused on theoretically and empirically exploring the influence of a composite's pore space characteristics and electrical properties on resistivity. There are three significant contributions of this work, each based on the following observations of (1) the absence of electrical flow through pore space at porosities less than a composite's porous percolation threshold, and (2) resistivity – porosity data in various sediments and rocks converge towards the theoretical lower Hashin-Shtrikman (HS) bound near the composite's critical porosities. The first significant contribution is the development of a tight empirical upper bound on the resistivity – total porosity relationship, where the upper bound is constrained by the percolation threshold at one end and by the critical porosity at the other. The upper bound is valid within the porosity range defined by the percolation threshold and critical porosity (Region II). The upper bound greatly reduces the range in possible resistivity values for a given porosity. The second significant contribution of this work is the development of a general equation that relates the internal geometry parameter and cementation exponent; both are empirical parameters in the resistivity – porosity relationship defined within the Region II porosity range. This relationship can be used to estimate one of the empirical parameters when the other can be constrained. The general relationship between the parameters is defined by a composite's critical porosity and the

primary constituent's grain sphericity. The third contribution of this work is insight into predicting a formation's pore space characteristics using resistivity – porosity data. Discussion on the influence of various pore space characteristics is based upon decades of published observations. Each of these contributions is valuable to both the environmental and petroleum industries for improving the characterization of aquifers and reservoirs, respectively.

Electrical resistivity measurements are controlled by the formation's channel porosity, whereas seismic velocity measurements are controlled by the formation's total porosity; thus the formation's channel porosity – total porosity relationship provides a link between resistivity and velocity. However, to date, minimal research has focused on relating resistivity and velocity. Our work focuses on theoretically and empirically exploring the relationship between electrical resistivity and seismic velocity. There are two significant contributions of this research. The first contribution is the development of upper and lower bounds on the electrical resistivity – seismic velocity relationship through their dependence on porosity. The resistivity – velocity bounds are simply created by combining resistivity and elastic moduli bounds at equal total porosities. These bounds can be used to constrain possible resistivity – velocity data pairs or to constrain the possible porosity range for a given data pair. The second contribution of this work is insight into constraining a formation's pore space characteristics using resistivity – velocity data. The real significance of these results is the potential for using known empirical relationships between resistivity and pore space characteristics to explain velocity trends and vice versa. With these results, electrical logs can be used to

better constrain seismic interpretations and develop more accurate maps of flow properties; a benefit to both the petroleum and environmental industries.

RESEARCH OBJECTIVES

The objective of this research has been to improve aquifer characterization. This objective was met by focusing on using rock physics theory and geophysical data to predict flow properties, such as porosity, permeability and clay content. The advantage of using geophysical data to predict these properties stems from the fact that geophysical data are less expensive and more spatially-abundant than lab- or field-measured, flow-property data. This research contributes three newly-developed relationships that significantly improve aquifer characterization: (1) a general relationship between total and channel porosities, (2) a general relationship between electrical resistivity and channel porosity, and (3) bounds on the electrical resistivity – seismic velocity relationship.

METHODS AND RESULTS

EXPLORATION OF DATA AND ROCK PHYSICS RELATIONS AT THE COLLABORATIVE FIELD SITE

This portion of the work was based on the fruitful collaboration with Dr. Frank Morrison, Dr. Yoram Rubin, and Dr. Jamie Rector from the University of California at Berkeley. The approach was to explore ways to enhance hydrogeological site characterization techniques by integration of geophysical imaging – with emphasis on borehole and surface-to-borehole seismic and electromagnetic techniques. A critical element of this work is a strong rock physics effort, which will provide the quantitative link between the geophysical observables, and the sediment and fluid properties that we need for the hydrogeologic interpretation.

One of the important issues in using rock physics to interpret seismic and VSP velocities is to understand the variations of velocity with lithology and clay content relative to the velocity variations with pore fluid saturations. Figure 1 on the left shows a lithology log at the well; the corresponding VSP velocities at two different offsets (10m

and 30m) are shown on the adjacent panels. Each panel plots the VSP velocity at different azimuth around the well. We do not see any strong azimuthal velocity variations. There is a marked increase in velocity just below the water table. Another interesting feature is the low velocity zone at about 37m depth. This low velocity zone shows up at both offsets. The HSU tops are not marked by any distinct changes in velocity across the boundary.

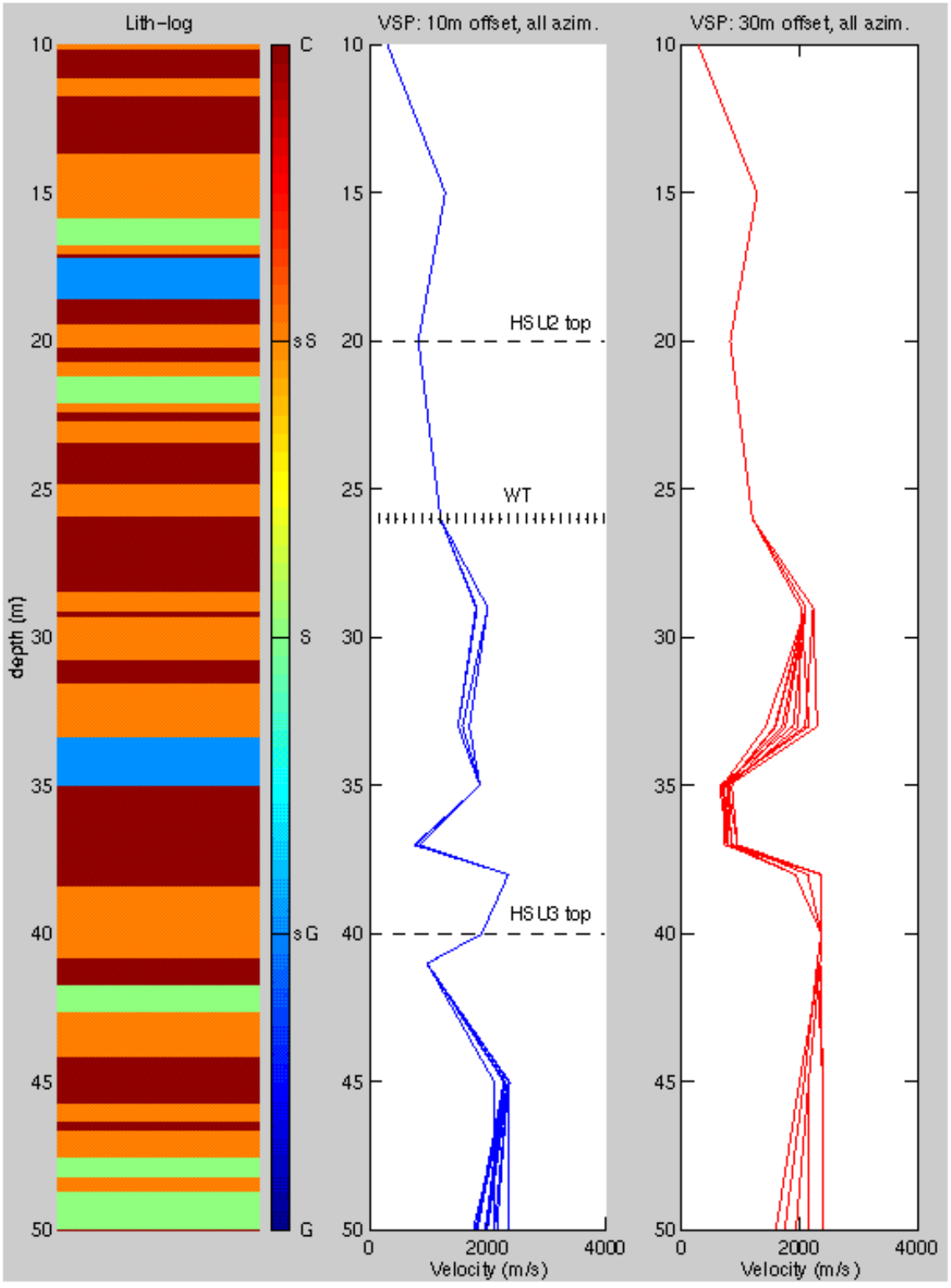
Lith-log
VSP: 10m offset, all azim.
VSP: 30m offset, all azim.
depth (m)
C
sS
S
sG
G
HS U2 top
WT
HS U3 top
Velocity (m/s)
Velocity (m/s)
10
15
20
25
30
35
40
45
50
0
2000
4000

Figure 1.

Figure 2 compares the VSP velocities for different lithologies (sands, clays, gravels, silty sands) with lab data on sediments. The data points are coded according to their position relative to the water table. The VSP velocities are comparable to the laboratory data, suggesting that laboratory derived velocity models (such as the Marion binary mixture model) may be applicable at this site. The velocities do not show a strong dependence on lithotype. In general velocities below the water table are higher than those above the water table, except for a few points. These correspond to a low velocity zone, and suggests the presence of an undersaturated region below the water table. The Hashin-Shtrikman upper and lower bounds (HS^+, HS^-) provide a simple yet robust indicator of undersaturation.

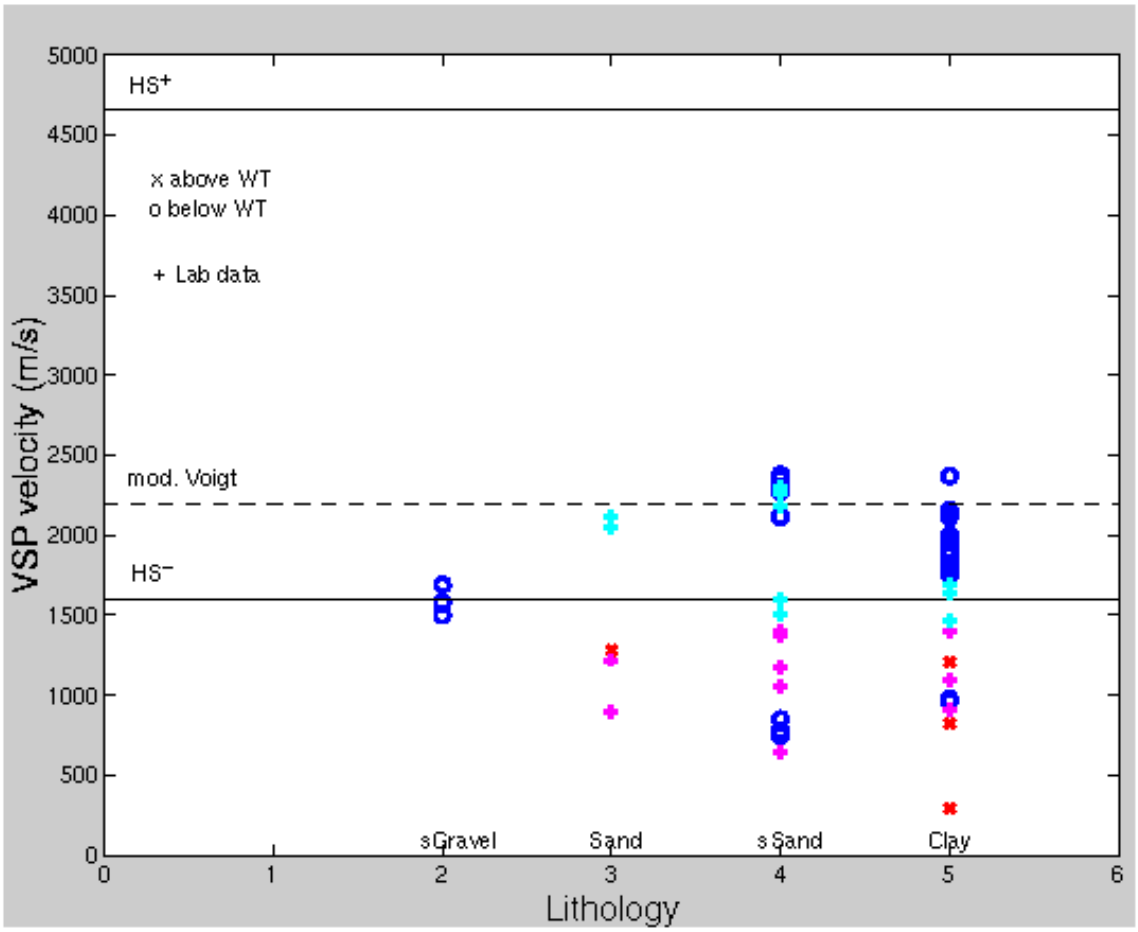

Figure 2

One of the goals was to test the impact of various seismic measurements on upscaling of rock physics relations between various properties such as velocity-porosity and velocity-clay relations. As a testing ground we build a synthetic model (Figure 3)

consistent with the shallow unconsolidated nature of the sediments at the site. The available well logs were used to assign distributions of physical properties to the different facies. The figure shows the facies distribution, the porosity, the related seismic velocity, and the resistivity. Care was taken to build the model in a self-consistent way taking into account the various relations between facies type, clay content, porosity, resistivity, and velocity.

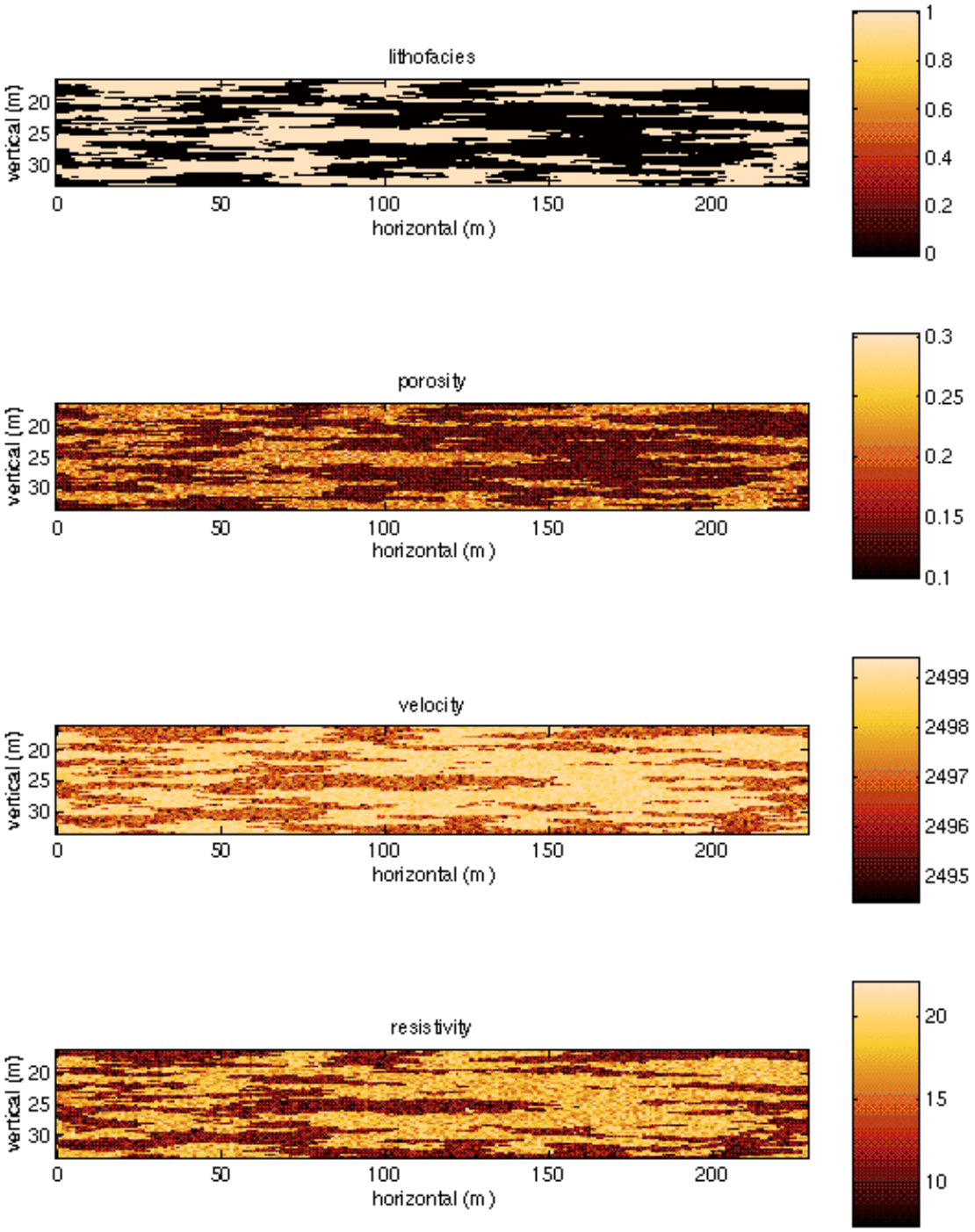

Figure 3.

Figure 4 shows the basic velocity-porosity relation used to define the seismic velocities in the earth model. The velocity-porosity relation is based on the Hamilton-Bachman regression which was derived for unconsolidated ocean bottom silty sand and

shale sediments. The figure also shows the modified Voigt and Raymer-Hunt-Gardner trends which are more appropriate for well-consolidated sediments, and have been used successfully in the oil and gas energy industry.

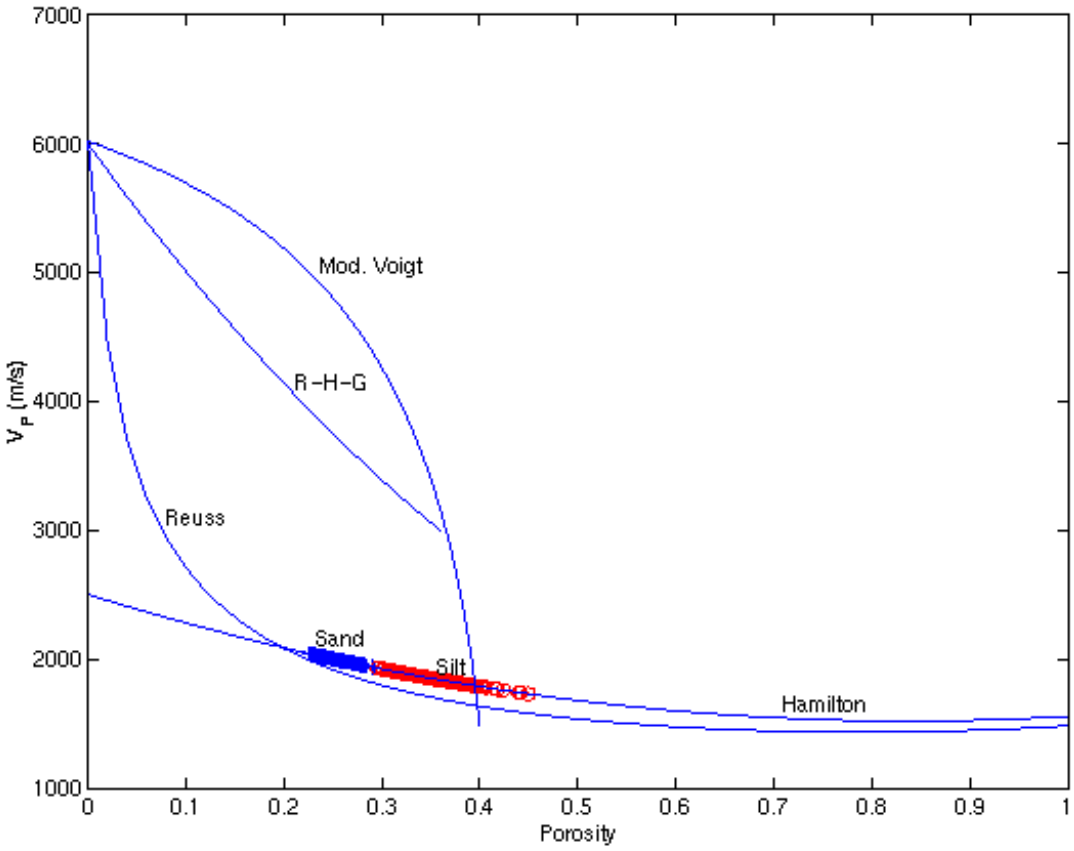

Figure 4

Once we had a consistent earth model we simulated a surface seismic image using a single scattering, frequency domain, Born filter approximation. Figure 5 shows the 'true' velocity model (top), and the observed seismic image (bottom).

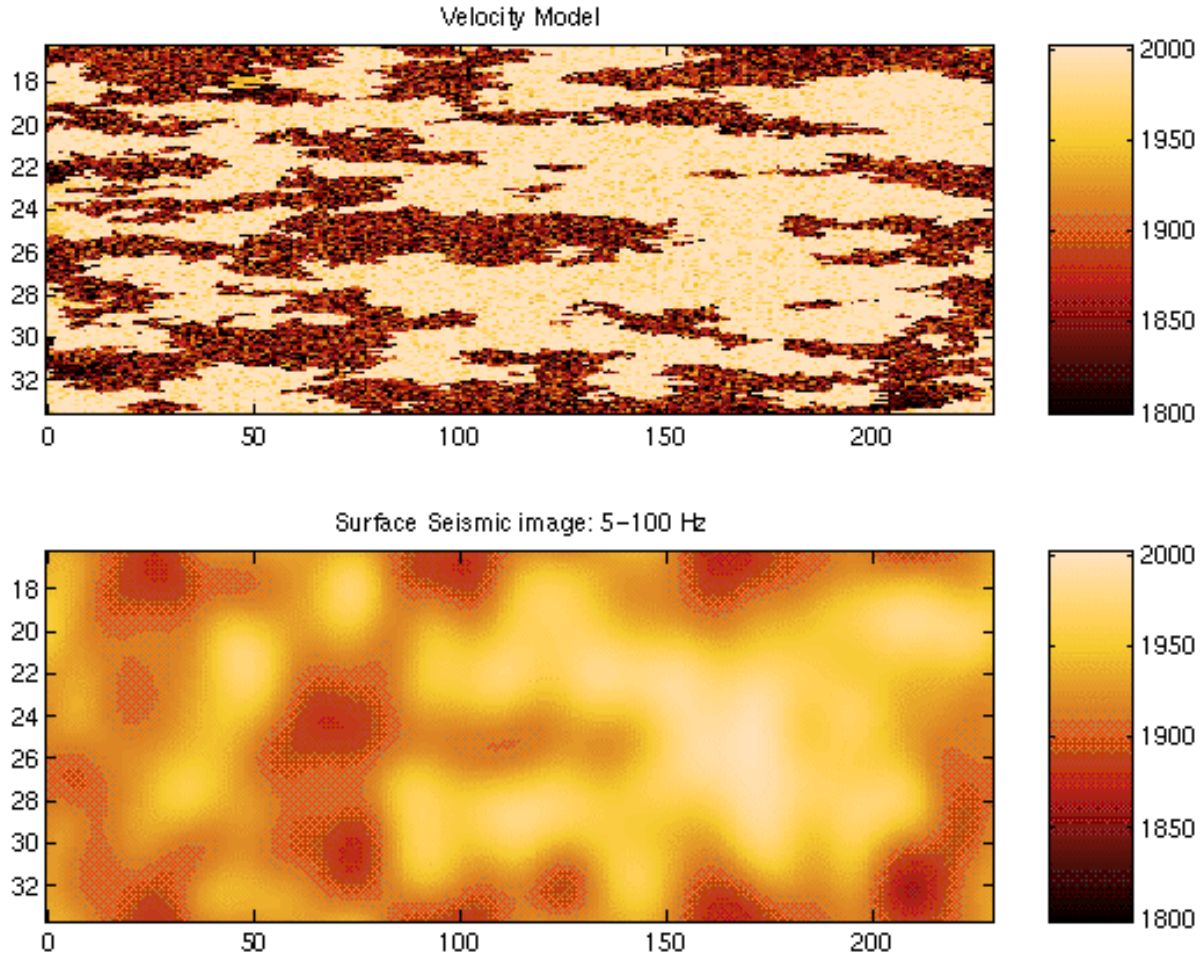
Velocity Model
18
20
22
24
26
28
30
32
0
50
100
150
200
2000
1950
1900
1850
1800
Surface Seismic image: 5–100 Hz
18
20
22
24
26
28
30
32
0
50
100
150
200
2000
1950
1900
1850
1800

Figure 5

Velocity-porosity and Velocity-clay relations which may be perfectly correlated at a fine scale can appear to have large scatter when imaged at a coarser scale. Figure 6 on the top left shows the velocity-clay relation for a dispersed binary mixture model of shaly sand sediments (the Marion model). The other panels show the scatter indroduced in this bilinear curve by the image response function of seismic measurements. On top right is the velocity-clay scatter plot obtained from the velocities imaged by an ART traveltime tomographic technique. On the lower row we see similar scatter from velocities in images synthesized by the Born filter, and another approximate pie filter in the spatial frequency domain. Thus taking the velocities obtained in any tomographic inversion and directly applying a deterministic transformation (such as the Marion model) to estimate sediment properties can lead to errors. It is necessary to take into account the scatter introduced by the image response of the measurement.

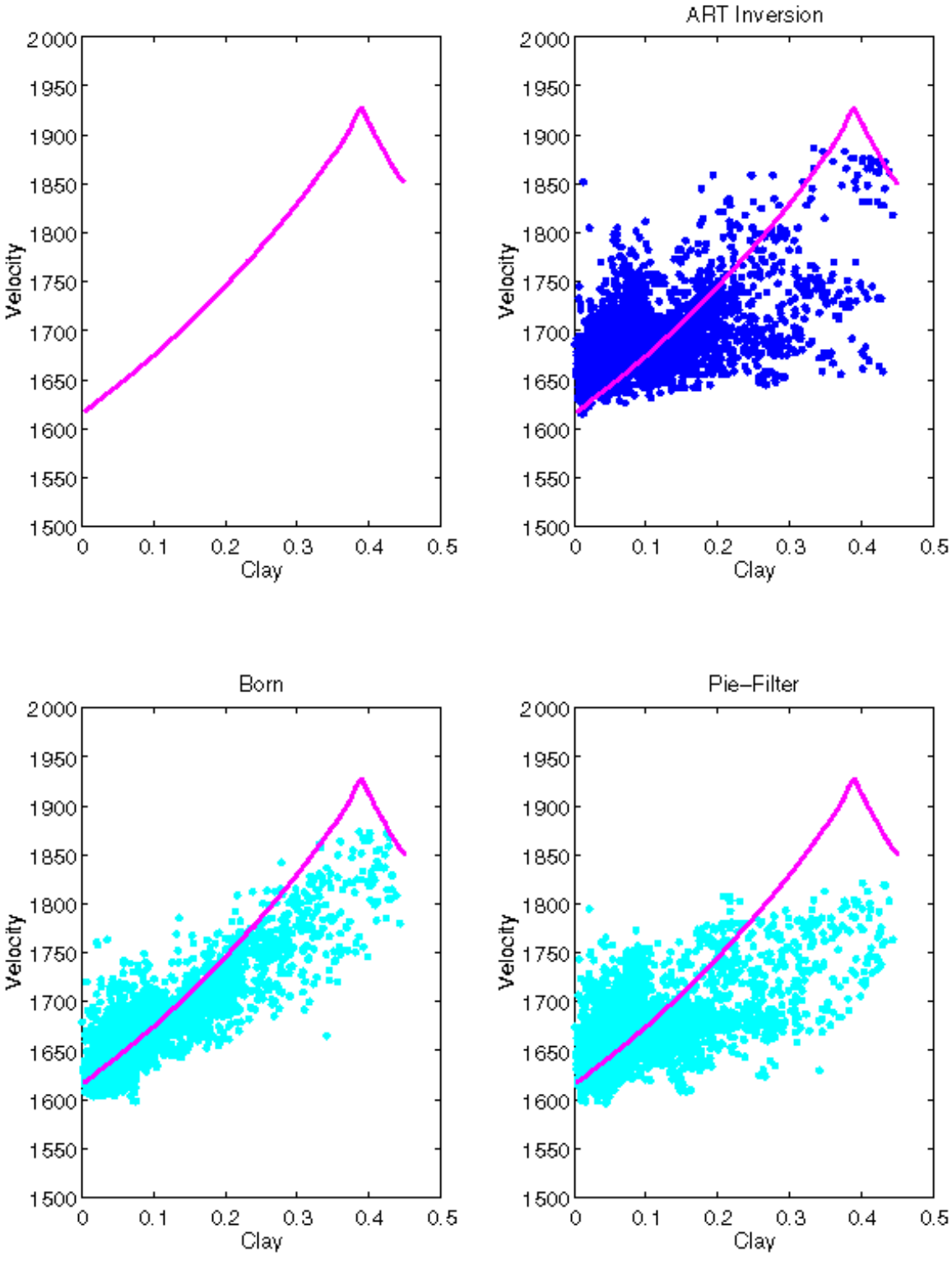
ART Inversion
Born
Pie–Filter
Velocity
Clay
2000
1950
1900
1850
1800
1750
1700
1650
1600
1550
1500
0
0.1
0.2
0.3
0.4
0.5

Figure 6

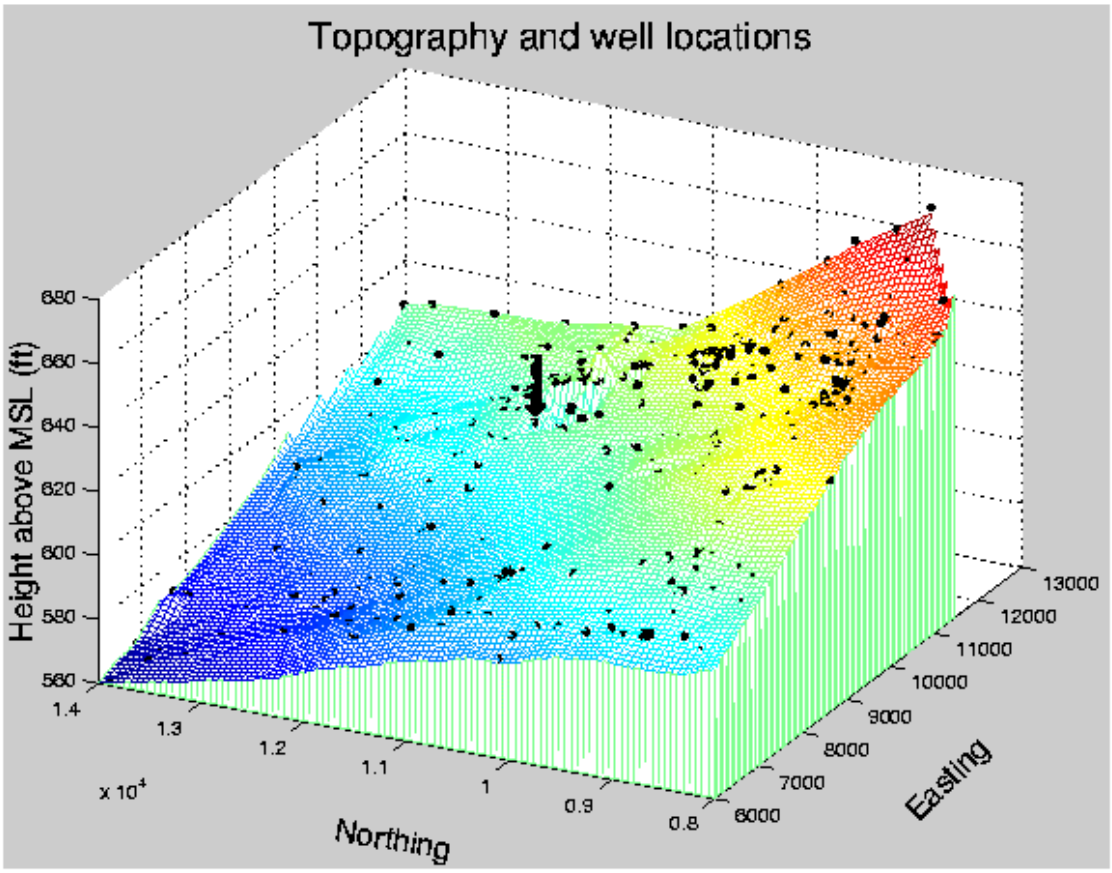

Figure 7

Figure 7 shows the topography of the LLNL remediation site with well locations. The well in the center is one of the wells where azimuthal VSP data has been acquired.

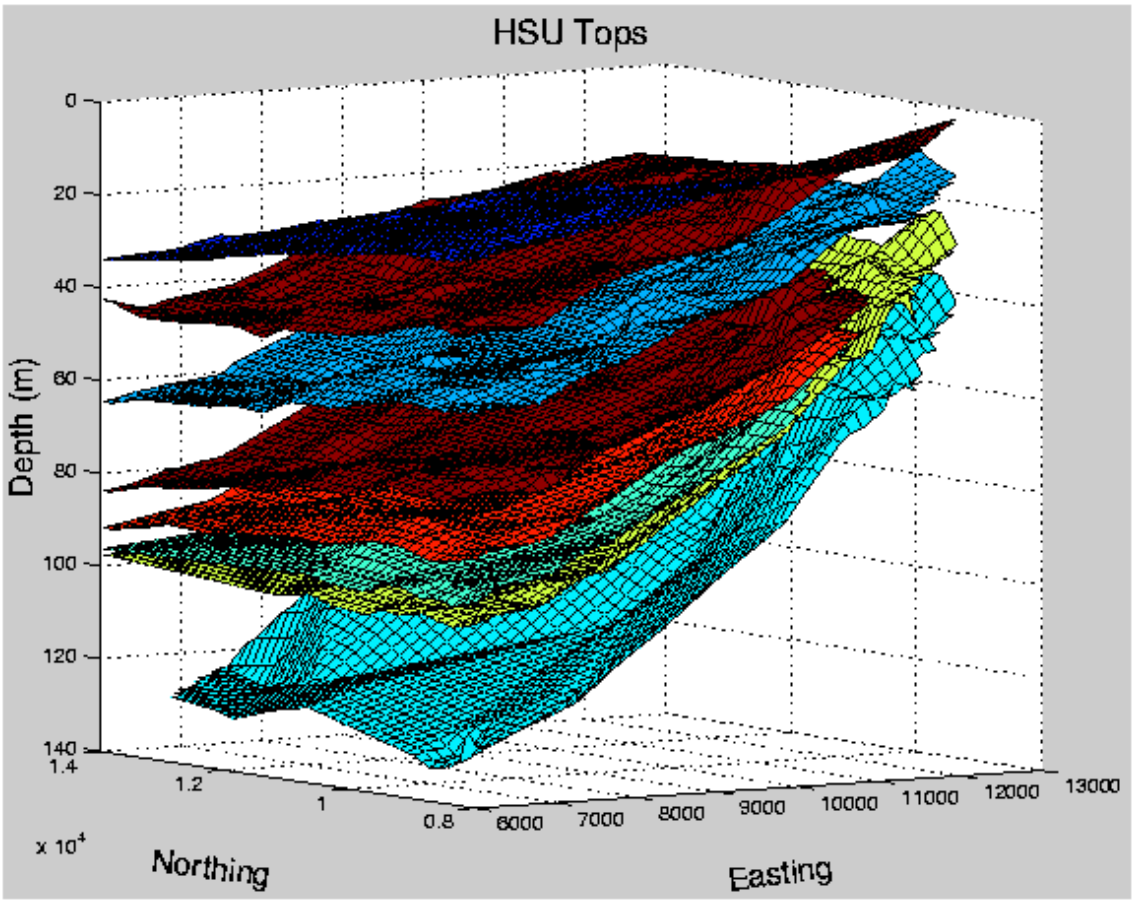

Figure 8

Figure 8 shows depths to the tops of the main subsurface hydrostratigraphic units (HSU) at the site.

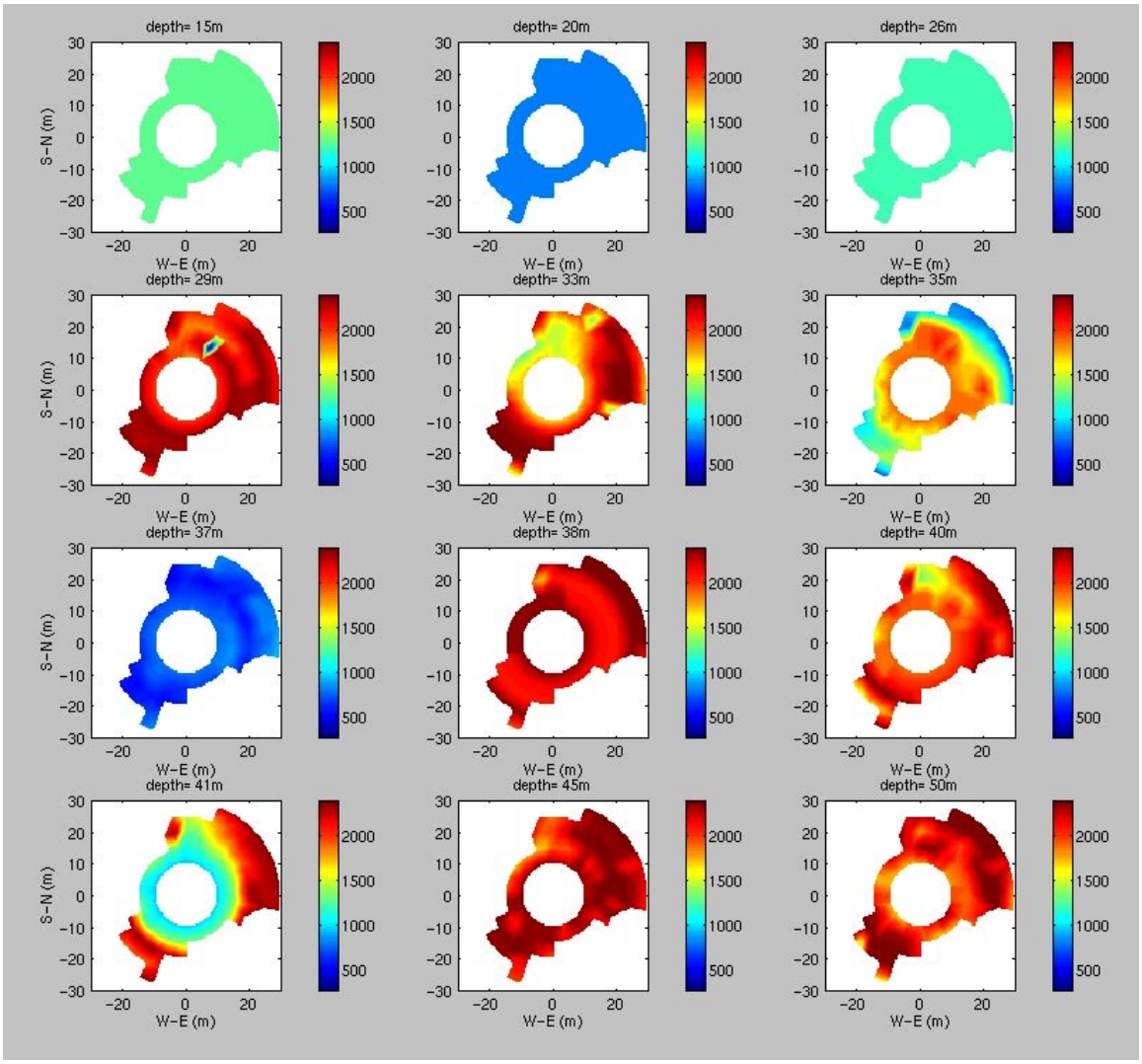

Figure 9

Figure 9 shows horizontal sections of the azimuthal VSP velocity data, slicing down from the top (upper left) to the bottom (lower right) of the data cube centered around the well. We see low velocities at the top (blues and greens), followed by a jump in the velocity (red) when the water table is encountered (second row). As we go deeper, a low velocity zone (blue) shows up around the well (third row).

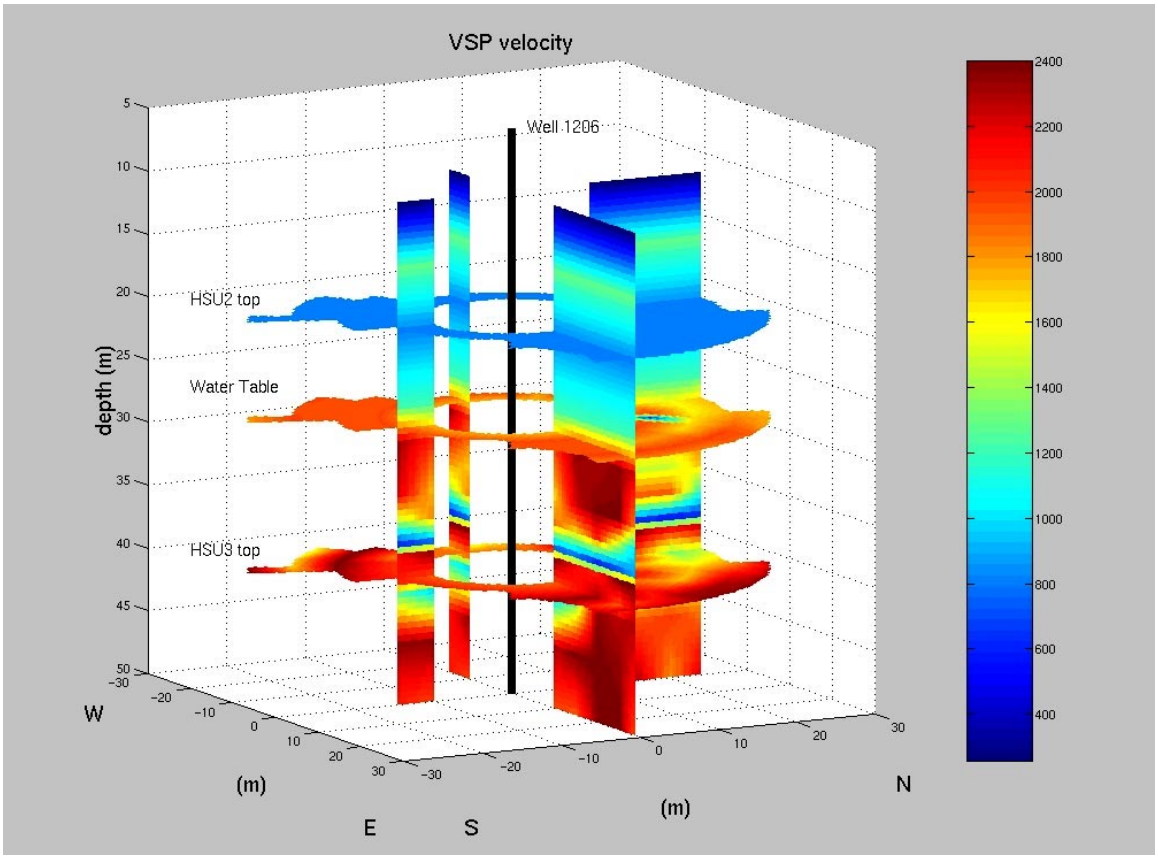

Figure 10

Figure 10 shows a 3-dimensional view of the well (center) and the P velocity around the well. The velocities along the tops of the two HSUs and the water table are also displayed. The water table is marked by the change from blue (lower velocity) to red (faster velocity). Below the water table we see the low velocity, possibly undersaturated zone around the well.

DEVELOPMENT OF BASIC ROCK PHYSICS RELATIONS FOR ELECTRICAL AND ACOUSTIC PROPERTIES OF SHALLOW SEDIMENTS

In this part of the project, we developed a method for bounding the relationship between formation resistivity factor F and compressional velocity V_p. This method constrains porosity by constraining possible ranges of F-V_p data. Both the petroleum and environmental industries would benefit from this technique because of the potential for using electrical logs to better constrain seismic interpretations and develop more accurate maps of flow properties. Our approach is simple. It involves combining the well-known Hashin-Shtrikman bounds for electrical conductivity and acoustic velocity and tracking porosity changes with the bounds. The significance of our approach is in its potential for using known relationships between formation factor and material properties in sediments and rocks to explain velocity trends and vice versa. We found that $F - \phi$ data in unconsolidated glass beads, and suspensions fall along the lower HS bound (Figure 11) and the $F - \phi$ values move up the lower HS bounds as a result of compaction and sorting while cementation moves the points away from the bound. Both resistivity and seismic velocity are significantly influenced by the same variables: pore structure (amount, texture and content), grain contacts (shape, sorting and cement degree and type) and clays (amount, type and distribution). Despite the complexity in the $F - \phi$ and $V_p - \phi$ relationships the electrical and acoustic Hashin-Shtrikman HS bounds can be combined at equal porosities to provide bounds on the $F - V_p$ relationship (Figure 12). The bold, solid line in Figure 12 represents the lower HS bounds and the curved, bold, dashed line represents the modified VoigtV_p upper bound. The vertical dashed line represents a suspension porosity limit. No $F - V_p$ data is feasible within the region marked by x's. Thus combining electrical and elastic data narrows the feasible region, constraining the possible sediment properties.

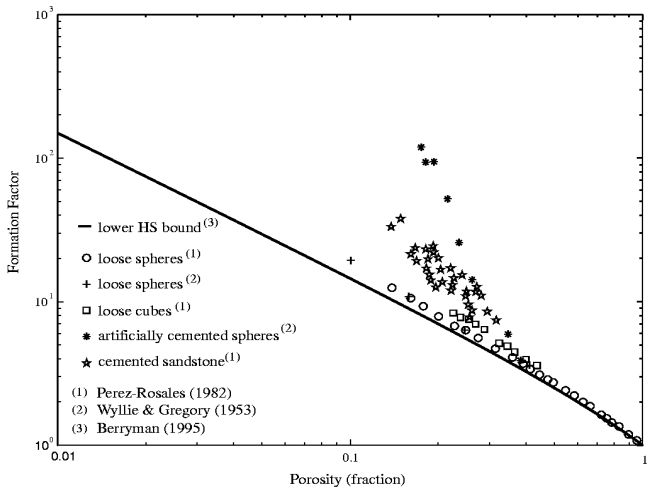

Figure 11.

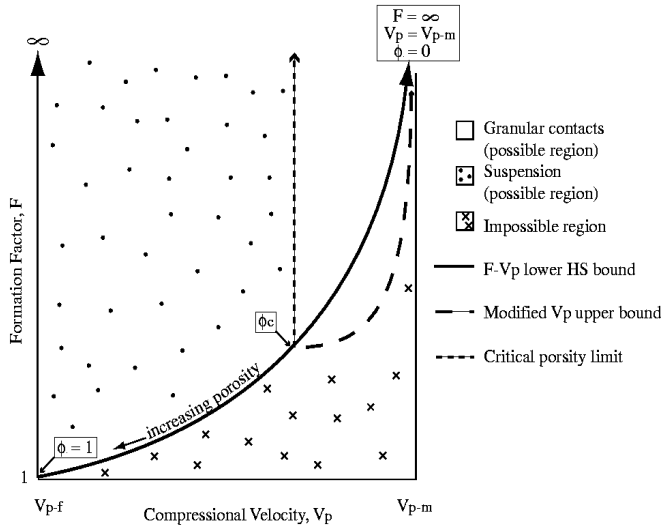

Figure 12

RELEVANCE, IMPACT, AND TECHNOLOGY TRANSFER

The results of this project apply directly to the technology needs of DOE's environmental management program. Geophysical methods, such as seismic and electrical imaging, provide a means to image the subsurface with a combination of resolution and volumetric coverage not possible by any other means. The results of this project allow for improved interpretation of these geophysical images, in terms of

sediment pore space microstructure. Of course, geophysical images cannot replace drilling, sampling, and well flow-testing, but they provide powerful and cost-effective complementary information.

The results can, in principle, be applied to any field or laboratory study where determination of flow properties is important, and where conditions are amenable to the collection of geophysical images.

We expect that these and similar results will eventually become a routine part of geophysical site characterization. Our results reported at scientific meetings usually generated substantial interest by both researchers and practitioners in environmental work.

PROJECT PRODUCTIVITY

The project met and exceeded our initial research goals. The collaboration with colleagues at UC Berkeley early in the project, allowed us to conclusively determine that low seismic velocity anomalies could only be explained by undersaturation. The subsequent work by those colleagues on field electrical imaging reinforced the need to improve our rock physics understanding of how sediment flow properties are related to seismic and electrical properties.

While the project stayed essentially on schedule, we requested and were granted a no-cost extension to allow for completion of a Ph.D. dissertation that was tied to the project.

PERSONNEL SUPPORTED

Gary Mavko, PI; Manika Prasad, Research Associate; Bill Waite, Post-doc;

Madhumita Sengupta, Yuguang Liu, Rubina Sen, Per Avseth, Wendy Corona, and Wei Chen, as graduate students .

PUBLICATIONS

Publications resulting from this work included:

Wempe, W. L., 2000, Predicting flow properties using geophysical data: Improving aquifer characterization, Ph.D. dissertation, Stanford University.

Wempe, W. and Mavko. G., The Electrical Resistivity - Acoustic Velocity Relationship: a method for constraining porosity, "SAGEEP Proceedings". Expected February 2000.

Wempe, W. and Mavko, G., The Propagation of Errors in Archie's Water Saturation Equation: the influence of an a-m relationship. Presented at the Geological Society of America 1999 Conference. October 1999.

Corona, W.W. and Mavko, G., Predicting Clay Content and Porosity from Gamma-ray and Conductivity Logs. "SAGEEP Proceedings", March 1999.

INTERACTIONS

Interaction with other workers and agencies during this project included the following:

a. Presentation of the results at international meetings, such as the Geological Society of America and SAGEEP.

b. Presentation of results at the 1999 and 2000 annual EMSP national workshops.

c. Collaboration with our colleagues at the University of California at Berkeley.

TRANSITIONS

The results of this work are directly applicable to many aspects of geophysical data interpretation, aimed at shallow environmental problems. The results are being incorporated into the teaching materials that we present to our graduate students at Stanford University. We also intend to propose follow-on projects building on the new results, to the DOE and other potential funding agencies.

PATENTS:

No patents were filed as a result of this project.

FUTURE WORK

The future work that we hope to pursue includes further refinement and validation of the resistivity and seismic relations developed in this project. In particular, we plan to continue exploring the relations of formation factor and velocity to pore microstructure, including grain size, sorting, angularity, compaction, and cementation. Ultimately, these will allow us to more effectively combine qualitative geologic information with more quantitative rock physics theory to optimally interpret geophysical data from hydrologic field sites.

APPENDICES – TECHNICAL DETAIL ON THE RESULTS AND METHODS OF THE PROJECT

A. THE CHANNEL POROSITY – TOTAL POROSITY RELATIONSHIP DEFINED PHYSICALLY, HYDRAULICALLY, ELECTRICALLY, AND ELASTICALLY

Background

Background on Defining Porosity Type

The total (or absolute) porosity ϕ is the sum of the channel ϕ_{ch} (or effective, or flowing, or free), trapped ϕ_{tr} (or stagnant, or residual) and isolated ϕ_i (or vuggy) porosities (Figure A1a).

$$\phi = \phi_{ch} + \phi_{tr} + \phi_i \tag{A1}$$

Total porosity can be measured in the lab using granular density data or estimated in the field using sonic or density logs. The channel porosity, the pore volume available for electrical and hydraulic flows, can be measured in the lab using helium or mercury injection or estimated in the field using electrical techniques. Trapped and isolated porosities are very difficult to measure directly, but can be estimated in the lab using grain density and channel porosity data. Isolated porosity, however, is insignificant in most clastic sediments ($\phi_i \approx 0$), with the exception of those with shale fragments or basalt-derived grains.

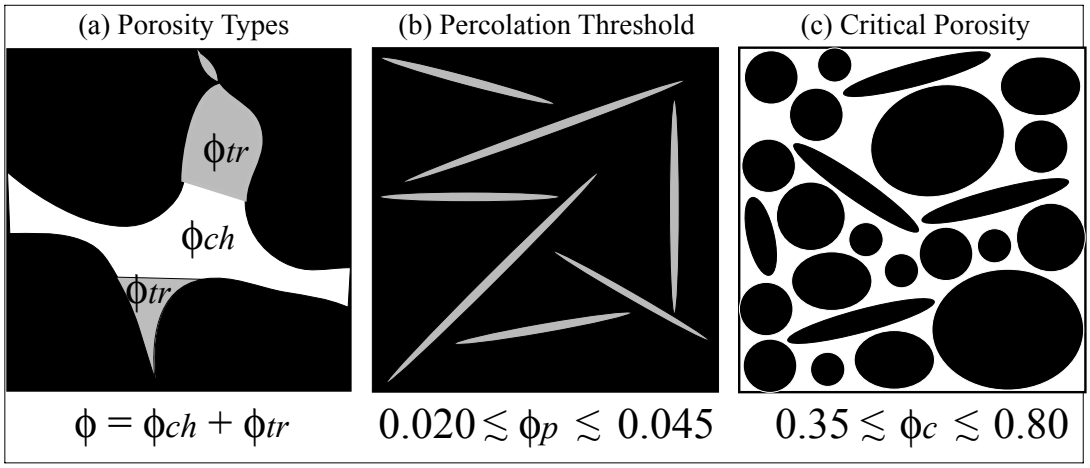

Figure A1: Pore space schematics. Schematic of (a) porosity type, (b) porosity percolation threshold and (b) granular critical porosity. Channel (white), trapped (gray) and isolated (gray) porosities. Granular region is shown in black.

As demonstrated in Figure A2, there is an apparent dependence of a clastic sediment's total porosity range on grain size; i.e. gravels have a narrower and lower porosity range than clays. The high porosity limit of a sediment's total porosity range, also known as critical porosity (discussed in the next section), occurs when the grains are randomly-oriented and loose. The low porosity limit, on the other hand, occurs when the same grains are packed as tightly as physically possible.

In nature, different grains weather differently depending on their mineralogy, thus have different characteristic shapes and sizes. Grain shape can be defined by its sphericity, roundness and texture. The sphericity of sand-size and smaller grains is mainly a function of the original mineral form, whereas the sphericity of pebble-size and larger grains is mainly a function of the transport process and duration (Boggs, 1987). The roundness of sand-size and smaller grains is primarily a function of mineralogy; i.e. hard quartz sand grains are rounded less readily than soft feldspar sand grains during transport. And, pebble-size and larger grains tend to be more easily rounded than smaller ones (Boggs, 1987). Regardless of mineralogy, however, small grains have larger specific surface areas, thus greater cohesive forces (Gueguen and Palciauskas, 1994) than large grains.

In summary, in a system of randomly-oriented loose grains, small platy grains (i.e. clays) have a higher porosity limit than a system of larger more spherical ones (i.e. eolian

sands). In a system of well-sorted grain pack, platy grains have greater available grain-to-grain contact area, therefore can reach tighter packing than a system of more spherical grains.

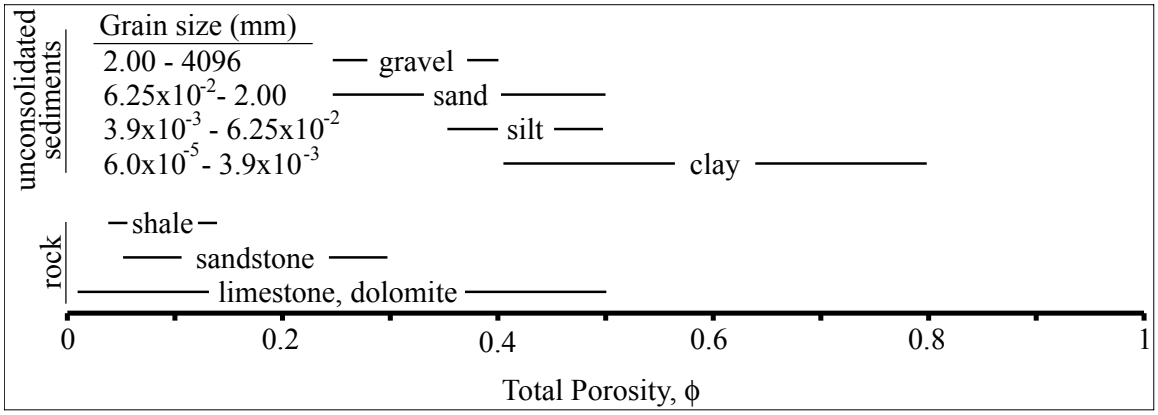

Figure A2: Observed total porosity ranges and grain size classes. Observed total porosity ranges for unconsolidated sediments and sedimentary rocks (Freeze and Cherry, 1979). Also shown are the ranges in grain sizes for gravel, sand, silt and clay grain-size classes (Boggs, 1987).

Percolation Threshold Theory Background

Extensive theory has been developed to define the inclusion volume fraction at which randomly oriented inclusions, whether pores or grains, are no longer connected; this volume fraction is known as the inclusion percolation threshold f_p (Webman et al, 1976, 1977; Straley, 1978; discussed in Gueguen and Palciauskas, 1994). The porous percolation threshold ϕ_p is defined by the porosity at which the pores are no longer connected; at $\phi < \phi_p$, $\phi = \phi_{tr}$ and $\phi_{ch} = 0$. The granular percolation threshold ϕ_c, also known as critical porosity, is the porosity at which grains are in suspension; at $\phi > \phi_c$, $\phi = \phi_{ch}$ and $\phi_{tr} = 0$.

The inclusion percolation threshold can be defined solely in terms of the inclusion depolarizing factor L_i of each principal axes i of the ellipsoidal inclusion. The depolarizing factors are functions of the ellipsoid length ratios between the principal axes (Landau and Lifshitz, 1960; Mendelson and Cohen, 1982), but they are not functions of the inclusion size itself. The depolarizing factors are constrained by

$$0 \le L_j \le 1 \qquad \text{(A2)}$$

$$L_1 + L_2 + L_3 = 1$$

For the special case of spheroidal inclusions (L_2=L_3) (Landau and Lifshitz, 1960) the depolarizing factors can be simplified to a general depolarizing factor term L where

$$L = L_1 \text{ and } L_2 = L_3 = \tfrac{1}{2}(1 - L) \tag{A3}$$

Landau and Lifshitz (1960) showed that the general depolarizing factor L is a function of the inclusion eccentricity e, where $e = \left|1 - \alpha^2\right|^{1/2}$. The inclusion aspect ratio α is equal to the ratio of the axis of symmetry b_2/b_1 where b_1 and b_2 are lengths in x_1 and x_2 directions. For prolate spheroids, $\alpha < 1$ (approaching disk-shape) and

$$L = \frac{1 - e^2}{2e^3}\left(ln\frac{1+e}{1-e} - 2e\right) \tag{A4}$$

For oblate spheroids, $\alpha > 1$ (approaching needle-shape) and

$$L = \frac{1 - e^2}{e^3}\left(e - \tan^{-1} e\right) \tag{A5}$$

For spheres, α= 1 and L = 1/3. Norris et al (1984) showed that the percolation threshold of spheroids can be expressed as

$$f_p = 1 - \frac{(1+L)(1+3L)}{1+9L} \tag{A6}$$

The inclusion percolation threshold f_p, the inclusion volume fraction at which inclusions become disconnected, is 1/3 for spherical, 1/5 for disk-shaped, and 0 for needle-shaped inclusions. Both the porous percolation threshold ($\phi_p = f_p$) and the granular percolation threshold (ϕ_c = 1 - f_p) can be determined experimentally using electrical techniques.

The porous percolation threshold ϕ_p is defined in a system of insulating grains and conductive fluid by the porosity at which an electrical current does not transmit through the pore space. The hydraulic percolation threshold occurs at very low porosity fractions in natural rocks; 0.025 in Fontainebleau sandstone, 0.035 in fused glass beads, and 0.045 in hot-pressed calcite (Mavko and Nur, 1997). According to percolation theory, these results suggest that pores are nearly needle-shaped at very low porosities. Sen et al (1981) and Webman et al (1975) found $0.135 \le \phi_c \le 0.250$ using a modified Archie's equation (Eqn. B13) and numerical modeling.

The granular percolation threshold ϕ_c is defined in a system of conductive inclusions (representing grains) and insulating fluid by the granular volume fraction at which the grains become suspended and an electrical current does not transmit through the granular system. Nur et al (1995) demonstrated the influence of ϕ_c on elastic properties; acoustically derived ϕ_c values range between 0.40 and 0.65 for various unconsolidated materials (Mavko et al, 1998). ϕ_c likely decreases in a material as a result of increased grain sphericity and grain smoothness. Even though sediments are grain-supported in static environments, not suspended, the ϕ_c of a material provides *tremendous* insight into the electrical resistivity – porosity and acoustic velocity – porosity relationships.

Background on Channel Porosity – Total Porosity Relationships

Since hydraulic permeability is a function of channel porosity, several authors have developed relationships to convert between total and channel porosities. Gal et al (1998) used lab-measured total and trapped porosity data (Figure A3) in the Fontainebleau sandstone (Bourbie and Zinszner, 1985) to derive the following empirical relationship

$$\phi_{ch} = 1.3486(\phi - 0.021)^{1.4} \tag{A7}$$

As seen in Figure A3, according to Eqn. A7, $\phi_{ch} \approx 0$ for $\phi < 0.021$ and $\phi_{ch} \approx \phi$ at $\phi \approx 0.54$. Perez-Rosales (1982), however, discussed the relationship between total and channel porosities in terms of the total porosity term in Archie's equation (Eqn. B13).

$$\phi_{ch} = \phi^m \tag{A8}$$

The cementation exponent m is high in composites where the pore space is discontinuous and disconnected, which translates to high amounts of ϕ_{tr}, where $\phi_{tr} = \phi - \phi_{ch}$. According to Eqn. A8, however, channel porosity should exist at porosities less than the composite's percolation threshold ϕ_p (Figure A3) and trapped porosity should exist even when grains are in suspension ($\phi > \phi_c$) (Figure A4), neither of which is observed.

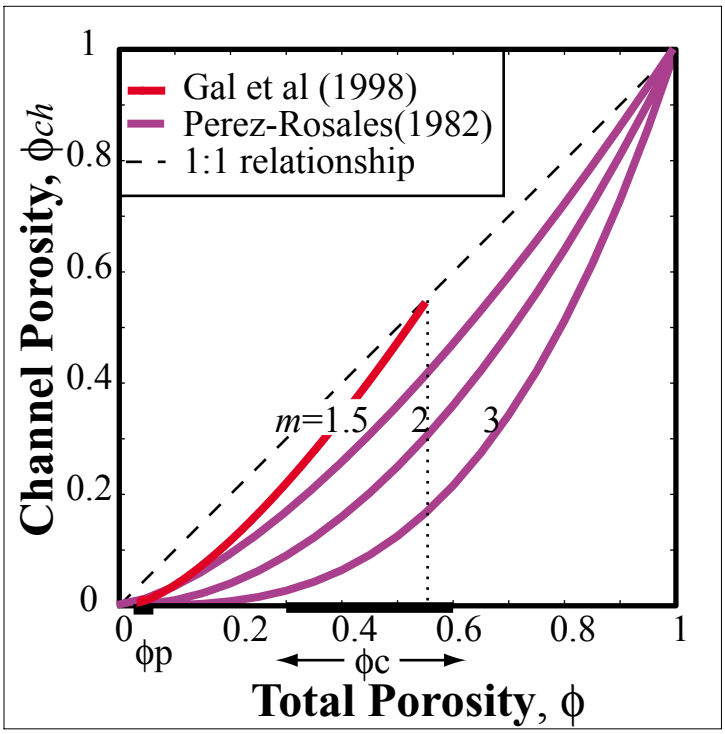

Figure A3: Channel and total porosities from previous work. Channel and total porosities according to Perez-Rosales (1982) (Eqn. A8)and Gal et al (1998) (Eqn. A7).

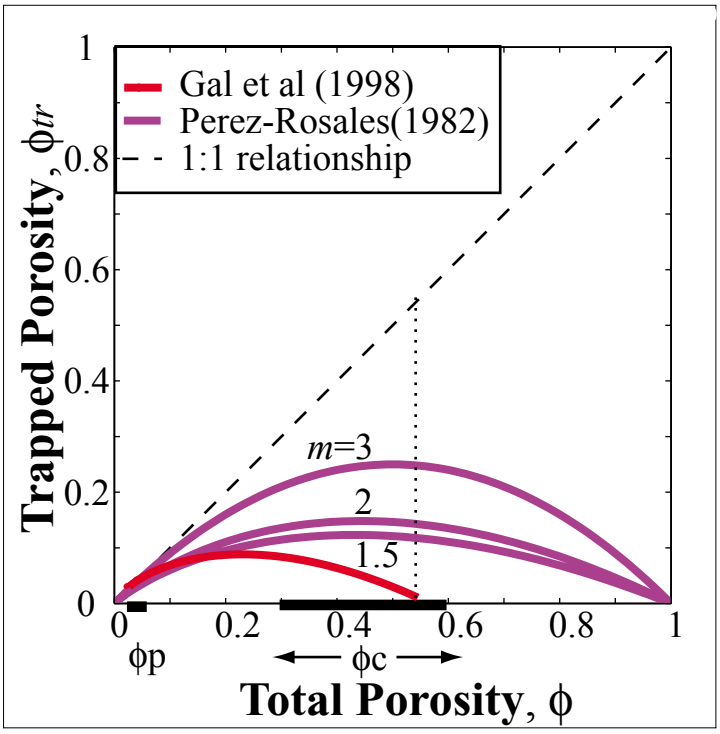

Figure A4: Trapped and total porosities from previous work. Trapped and total porosities according to Perez-Rosales (1982) (Eqn. A8) and Gal et al (1998) (Eqn. A7).

Sen et al (1979) suggested modifying the porosity term in Archie's equation to account for the percolation threshold by $(\phi - \phi_p)^m$. If the porosity term in Archie's equation is equal to the channel porosity like Perez-Rosales (1982) suggested, then the channel porosity could be expressed as

$$\phi_{ch} = (\phi - \phi_p)^m \tag{A9}$$

The modification of the porosity term made by subtracting the percolation threshold is similar to the modification in the Kozeny-Carman equation for permeability by Mavko and Nur (1997), which is of the form $(\phi - \phi_p)^x$. The percolation threshold term in Eqn. A9 has a minimal effect on ϕ_{ch} at high ϕ values.

New Results on the Channel Porosity – Total Porosity Relationship

Three Distinct Porosity Regions Defined Physically, Hydraulically, Electrically and Acoustically

The granular and porous percolation thresholds together define three distinct porosity regions physically, hydraulically, electrically and elastically. Physically, these three porosity regions are defined by the amounts of channel porosity ϕ_{ch} and trapped porosity ϕ_{tr}. Hydraulically and electrically, the regions are defined by the ability for fluid and currents to flow through the pore space. Acoustically, the regions are defined by the pore space stiffness and rigidity that contributes to the system as a whole.

Region I is defined for porosities less than the porosity percolation threshold ($\phi < \phi_p$), where the pore space is no longer connected ($\phi_{ch} = 0$); all of the porosity is trapped ($\phi = \phi_{tr}$ from Eqn. A1). Electrical currents and fluids cannot flow through a system's pore space if porosities are lower than the percolation threshold since the pores aren't connected; in other words the system's formation resistivity factor immediately approaches infinity and the hydraulic permeability equals zero. Since fluids cannot escape from the pore space when an acoustic wave travels through the system (the system's pore pressure gradients are "unrelaxed"), the pore space is relatively stiff; the moduli of such low porosity materials are approximately equal those of the mineral constituent.

Region II is defined for porosities in between the porous percolation threshold and the critical porosity ($\phi_p \leq \phi \leq \phi_c$), where the total porosity is connected but trapped porosity exists ($\phi = \phi_{ch} + \phi_{tr}$ from Eqn. A1). Since not all of the porosity is available for flow in this region, the abilities for electrical currents and fluids to flow depend on the amount of trapped porosity. The amount of trapped porosity depends on the formation's pore space characteristics; i.e. sorting, cementation, compaction and dispersed clay content. These same pore space characteristics control the empirical, formation-specific parameters B in the Kozeny-Carman relation for permeability (Mavko and Nur, 1998) and a_H and m in the Humble equation (Eqn. B13) for formation factor (Table A1). These pore space characteristics also influence the system's stiffness K, rigidity μ and density ρ; hence

they influence the system's acoustic velocities (Table A1). The influences of these pore space characteristics on the ϕ_{ch} - ϕ relationship are discussed later.

Region III is defined for porosities greater than the critical porosity where grains are in suspension and all of the pore space is not only connected, but is also available for flow ($\phi_{tr} = 0$, so $\phi = \phi_{ch}$ from Eqn. A1). Since all of the porosity is available for flow, the permeability is infinite and the formation factor only depends on the total porosity (Table 2.1), not on other properties such as sorting, clay content, or grain shape. A system of suspended grains lacks rigidity ($\mu = 0$) and is highly compressible (low K), therefore in this region, the effective bulk modulus K is dominated by the fluid modulus K_w.

Region	Porosity Range	Permeability	Resistivity	P-wave Velocity
I	$0 \le \phi < \phi_p$	0	$f(R_m)$	$f(V_{p\text{-}m})$
II	$\phi_p \le \phi \le \phi_c$	$f(\phi, B)$	$f(\phi, a_H, m)$	$f(\phi, K_i, \mu_i, \rho_i)$
III	$\phi_c < \phi \le 1$	$f(\phi, B)$	$f(\phi, R_i)$	$f(\phi, K_i)$

Table A1: Three distinct porosity regions defined hydraulically, electrically and elastically. Defined by the percolation threshold ϕ_p and critical porosity ϕ_c.

New Channel Porosity – Total Porosity Relationship

As discussed in above, the percolation threshold ϕ_p and critical porosity ϕ_c define three distinct $\phi_{ch} - \phi_{tr}$ porosity regions (Table 2); $\phi_{ch} = 0$ in Region I, $\phi_{tr} = 0$ in Region III, and both ϕ_{ch} and ϕ_{tr} exist in Region II. This section focuses on developing a relationship that describes how ϕ_{ch} and ϕ_{tr} are controlled in the Region II ($\phi_p \leq \phi \leq \phi_c$), the porosity range of most rocks and sediments. In Region II, a composite's characteristic hydraulic permeability k and formation resistivity factor F are functions of the composite's channel porosity ϕ_{ch}, whereas its characteristic elastic moduli K and μ are functions of the composite's total porosity ϕ. The total porosity is the sum of channel and trapped porosities (Eqn. A1), assuming isolated porosity is negligible ($\phi_i = 0$). A composite's trapped porosity is a function of the pore space characteristics and can be described by Archie's exponent m. The $\phi_{ch} - \phi$ relationship, which is based upon the pore space characteristics, provides the link between k, F, K and μ; an extremely valuable link for groundwater, petroleum and geotechnical engineers.

From the discussion above, we know that the channel porosity is zero at the percolation threshold (the low porosity limit) and equal to the total porosity at the critical porosity (the high porosity limit). The porosity term proposed by Sen et al (1979) accounts for the low porosity limit, but as seen in Figure A4, it suggests that significant trapped porosity exists when the composite is a suspension, which does not meet the high porosity limit. The high porosity limit can be account for by multiplying Eqn. A9 by a formation-specific parameter A, which is defined by the composite's percolation threshold ϕ_p and critical porosity ϕ_c.

$$\phi_{ch} = A(\phi - \phi_p)^m \tag{A10}$$

$$A = \frac{\phi_c}{(\phi_c - \phi_p)^m} \tag{A11}$$

As seen in Figure A5, A significantly influences the ϕ - ϕ_{ch} relationship, especially at high porosities. Eqn. A10 is of the same form as that empirically derived by Gal et al

(1998) (Eqn. A7). The ϕ_p, ϕ_c and m values characteristic of the Fontainebleau sandstone can be solved for in Eqn. A7 by Eqn. A10; $\phi_p = 0.021$, $\phi_c = 0.54$, and m =1.4 (Figure A5).

Region	Porosity Range	Channel Porosity, ϕ_{ch}	Trapped Porosity, ϕ_{tr}
I	$0 \le \phi < \phi_p$	0	ϕ
II	$\phi_p \le \phi \le \phi_c$	$A(\phi - \phi_p)^n$	$\phi - A(\phi - \phi_p)^n$
III	$\phi_c < \phi \le 1$	ϕ	0

Table A2: Three porosity regions defined physically. Defined by the percolation threshold ϕ_p and critical porosity ϕ_c in terms of channel and trapped porosities.

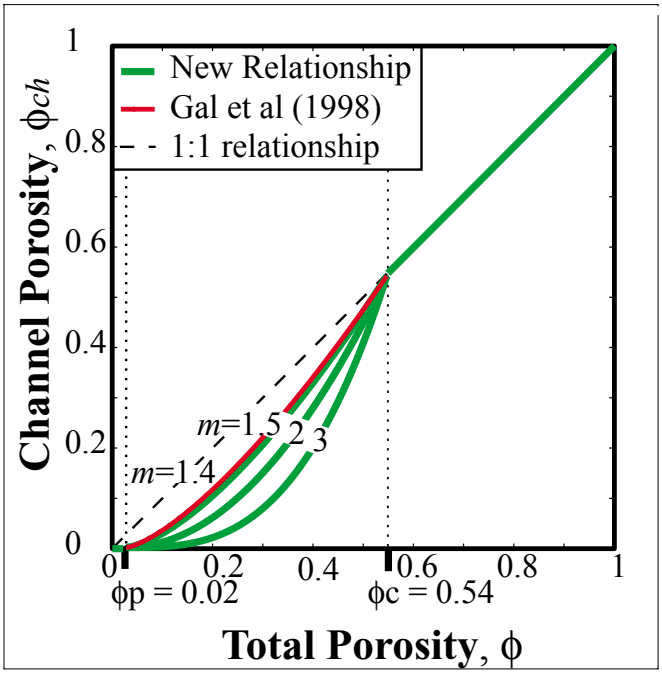

Figure A5: Channel and total porosities using new relationship. Channel and total porosities according to Eqns. A10 and A11 and Gal et al (1998) (Eqn. A7).

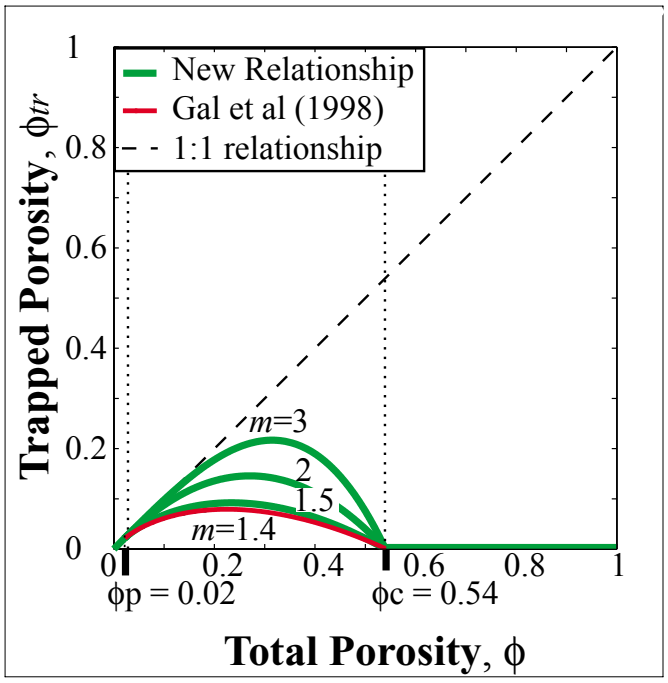

Figure A6: Trapped and total porosities using new relationship. Trapped and total porosities according to Eqns. A10 and A11 and Gal et al (1998) (Eqn. A7).

Insight into Empirical Parameters in Formation Factor and Permeability Equations

As discussed earlier, both formation resistivity factor F and hydraulic permeability k are controlled by the ability for electrical currents and fluids, respectively, to flow through a formation's pore space; the formation's channel porosity ϕ_{ch} defines the pore space available for flow. Forms of both the Humble (Winsauer et al, 1952) and the Kozeny-Carman (Kozeny, 1927 and Carman, 1937) equations are by far the most widely used empirical $F - \phi$ and $k - \phi$ relationships, respectively. Each relationship has formation-specific empirical parameters and a formation-specific exponential porosity term of the form of Eqn. A10.

Equation A10 suggests that the formation-specific A term is absorbed into the empirical, formation-specific a_H term in the Humble equation (Eqn. B14) modified by Sen et al (1979). In fact, later we show just that; a_H can be expressed as a function of A (Eqn. B19).

Mavko and Nur (1997) modified the porosity term in the Kozeny-Carman equation for permeability by subtracting the percolation threshold from the total porosity. The modification is of the form $(\phi - \phi_p)^x$, where $x \approx 3$ in cemented rocks. If it is assumed that $x \approx m$ in Eqn. A10, then the A term is likely adsorbed into the empirical, formation-specific parameter B in the Kozeny-Carman equation.

The Influence of Pore Space Characteristics on Channel and Trapped Porosities

In the porosity region $\phi_p \leq \phi \leq \phi_c$ (Region II), the channel porosity ϕ_{ch} and total porosity ϕ can be influenced by several pore space characteristics such as sorting, cementation, compaction, and dispersed clay volume. When a material of a given volume fills the pore space of a composite, the composite's total porosity decreases by an amount equal to the volume of the pore-filling material. The degree of influence of the pore-filling material on trapped and channel porosities, however, is defined by the parameter m in Eqn. A10. For example, in two different composites with the same total porosity, the trapped porosity of a poorly sorted composite will be less (low m value) than that in a cemented one (high m value) where pore throats become sealed and trapped. Decades of observations show that m tends to be largest when porosity decreases from cementation, smallest when it decreases from sorting and somewhere in between when it decreases from compaction and increased volume of pore-filling, dispersed clay. The influences of the pore space characteristics on the $\phi_{ch} - \phi$ relationship are shown in Figure A7.

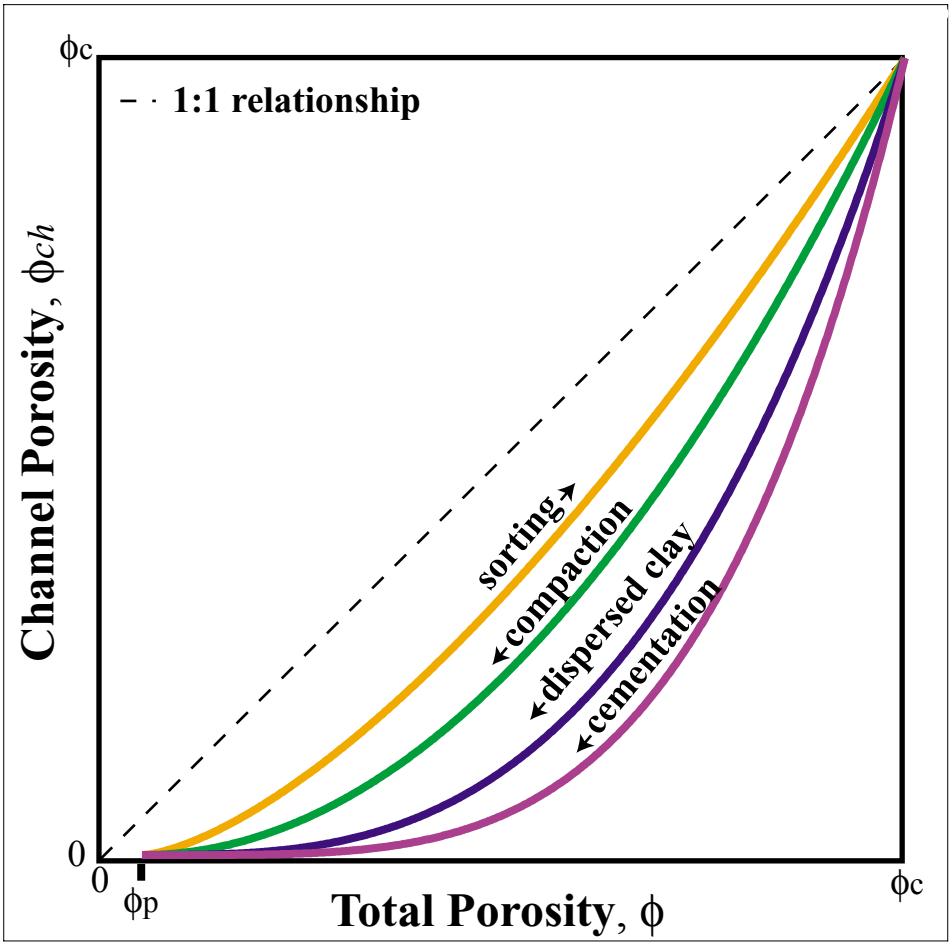

Figure A7: The influence of pore space characteristics on channel porosity. Arrows indicate increased sorting (reduced grain size distribution), compaction, pore-filling dispersed clay volume, and cementation.

Conclusions

- A formation's percolation threshold ϕ_p and critical porosity ϕ_c define three distinct porosity regions physically, hydraulically, electrically and elastically: $0 \leq \phi \leq \phi_p$ in Region I, $\phi_p < \phi < \phi_c$ in Region II, and $\phi_c \leq \phi \leq 1$ in Region III.

- A formation's trapped porosity ϕ_{tr} is controlled by the formation's pore space characteristics through Archie's exponent m.

- The $\phi_{ch} - \phi$ relationship for a formation is defined by the formation's characteristic ϕ_p, ϕ_c and m values.

- The formation-specific A term in the $\phi_{ch} - \phi$ relationship can be expressed solely as a function of ϕ_p, ϕ_c and m.

- The A term is adsorbed into the empirical, formation-specific parameters a_H and B in the Humble and Kozeny-Carman equations

References

Archie, G.E., 1942. The electrical resistivity log as an aid in determining some reservoir characteristics. *Trans. Am. Inst. Mech. Eng.,* 146, 54-62.

Bourbie, T., and Zinszner, B., 1985. Hydraulic and acoustic properties as a function of porosity in Fontainbleau sandstone. *J. Geophys. Res*., v. 90, 11,524 – 11, 532.

Boggs, S. Jr., 1987. *Principles of Sedimentology and Stratigraphy*. Merrill Publishing Company, Columbus, Ohio.

Carman, P.C., 1937. Fluid Flow through a granular bed. Trans. Inst. Chem. Eng. London, 15, 150 – 156.

Freeze, R.A. and Cherry, J.A., 1979. *Groundwater*. Prentice Hall, Englewood Cliffs, N.J.

Gal, D., Dvorkin, J., and Nur, A., 1998. A physical model for the porosity reduction in sandstones. *Geophys*., 63, 454 – 459.

Gueguen, Y., and Palciauskas V., 1994. *Introduction to the Physics of Rocks*. Princeton University Press, Princeton.

Kozeny, J., 1927. Uber kapillare Leitung des Wassers im Boden. Sitzungsber. Akad. Wiss. Wien., v. 136, 271 – 306.

Landau, L.D., and Lifshitz, E.M., 1960. *Electrodynamics of continuous media.* Oxford, Pergamon Press.

Mavko, G., and Nur, A., 1997. The effect of a percolation threshold in the Kozeny-Carman relation. *Geophys*., 1480 – 1482.

Mavko, G., Mukerji, T., and Dvorkin, J., 1998, *The Rock Physics Handbook: tools for seismic analysis in porous media*, Cambrige University Press.

Mendelson, K.S., and Cohen, M.H., 1982. The effect of grain anisotropy on the electrical properties of sedimentary rocks. *Geophys*., 47, 257 – 263.

Norris, A.N., Sheng, P., and Callegari, A.J., 1984. Effective-medium theories for two-phase dielectric media. *J. Appl. Phys*., 57, 1990 – 1996.

Nur, A., Mavko, G., Dvorkin, J., and Gal, D., 1995. Critical Porosity: The key to relating physical properties to porosity in rocks, in *Proc., 65th Ann. Int. Meeting, Soc. Expl. Geophys.*, 878.

Perez-Rosales, C., 1982, On the Relationship Between Formation Resistivity Factor and Porosity, *Soc. Pet. Eng. J.*, 531-536.

Sen, P.N., Scala, C., and Cohen, M.H., 1981. A self-similar model for sedimentary rocks with application to the dielectric constant of fused glass beads. *Geophys.*, V. 46, N. 5, 781 – 795.

Straley, J.P., 1978. Critical phenomena in resistor networks. *J. Phys.*, v. C9, 783 – 795.

Webman, I., Jortner, J., and Cohen, M.H., 1967. Numerical simulation of continuous percolation conductivity. *Phys. Rev.*, V. B14, 4737 – 4740.

Webman, I., Jortner, J., and Cohen, M.H., Numerical simulation of electrical conductivity in microscopically inhomogeneous materials. *Phys. Rev.*, v. B11, 2885 – 2892.

Webman, I., Jortner, J., and Cohen, M.H., 1977. Theory of optical and microwave properties of microscopically inhomogeneous materials. *Phys. Rev.*, v. B15, 5712 – 5723.

Winsauer, W.O., Shearin, H.M. Jr., Masson, P.H., and Williams, M., 1952. Resistivity of Brine-Saturated Sands in Relation to Pore Geometry. *Bull., AAPG*, 36, 2, 253-277.

B. DEVELOPMENTS IN THE ELECTRICAL RESISTIVITY – POROSITY RELATIONSHIP

Introduction

Electrical resistivity data are by far the most common geophysical data collected for environmental groundwater investigation. Since electrical currents respond to changes in a formation's electrical properties and pore-space characteristics, resistivity data are typically used to *qualitatively* interpret changes in fluid properties (i.e. freshwater versus contaminated water) and locate clay-rich formations. Resistivity data, however, can also be used *quantitatively* to estimate porosity and permeability. Channel porosity and permeability control hydraulic flow and are therefore the most important formation properties to estimate in order to characterize flow.

This section focuses on theoretically and empirically exploring the influence of a composite's pore space characteristics and electrical properties on resistivity. The most significant contributions of this work are the development of a tight upper bound on the formation factor – total porosity relationship, the generalization of the internal geometry parameter – cementation exponent relationship, and insight into determining formation pore space characteristics using formation factor – porosity data. A common problem encountered when analyzing resistivity – porosity data is determining formation-specific, empirical parameters a and m in the resistivity – porosity relationship. The developments within this section can be used to deal with such problems. These developments are valuable to both the environmental and petroleum industries for improving the characterization of aquifers and reservoirs.

A composite's electrical conductivity, the inverse of resistivity, is a measure of the ease for an electrical current to be transmitted (via electrons and ions) through the composite. Varying material properties are responsible for variations up to 20 orders of magnitude in the resistivity of sediments and rocks. The conductivity of a material is influenced by the conductivities of the mineral and fluid constituents and by the

composite's formation resistivity factor, the inability for electrical flow through the pore space. Both conductivity and formation factor are influenced by formation anisotropies. The majority of common minerals are insulators (i.e. feldspars and quartz) (Parkhomenko, 1967), however, ore and clay minerals are conductive. Fluids such as oil, freshwater and gas are resistive, whereas brines can be highly conductive. Besides the influence of their electrical properties, liquids may additionally increase the mobility of the surface ions on insulators that have strong adsorption characteristics (Parkhomenko, 1967). Electrically, most sediments can be simplified as one of two mineral-fluid systems: (1) insulating minerals and pore-filling fluid, or (2) insulating minerals, conducting clay minerals, and pore-filling fluid (liquid or gas). Even though the data acquisition frequency and formation anisotropies can significantly influence resistivity measurements, the discussion of these topics is beyond the scope of this work.

Mineral/Fluid	Resistivity (Ω-m)
Water	10^{-2} - 10^{2} (2)
Quartz	$10^{14} – 10^{16}$ (1)
Calcite	$5 \cdot 10^{14}$ (1)
Whetted Clay	$1 – 10^{3}$ (2)

Table B1: Resistivities of common sediment constituents. (1) Parkhomenko (1967); (2) Rider (1986)

Theoretical effective medium bounds on resistivity are functions of the constituent's conductivities and volumes, whereas theoretical effective medium approximations additionally require grain geometry information. Theory has not been developed to describe the influence of various pore-space characteristics, such as cementation and tortuosity, on conductivity. For comprehensive discussion of various theories refer to Berryman (1995) and Mavko et al (1998).

Empirical relationships are valuable for determining the relationship between resistivity and porosity when the composite' granular geometries and mineral constituents are unknown. Most empirical relationships require true (measured) conductivity and the conductive constituent's conductivity and volume fraction. The influence of various pore space characteristics is accounted for in empirical parameters. For a review of empirical

relationships refer to Tiab and Donaldson (1996), Schlumberger (1989) and Worthington (1985).

Background

Theoretical Resistivity Background

Hashin-Shtrikman Bounds

The theoretical Hashin-Shtrikman (HS) bounds for electrical conductivity (Hashin and Shtrikman, 1962) provide upper and lower limits for the resistivity-porosity relationship in a multi-constituent media. The upper HS bound on resistivity R_{HS+} is equal to the inverse of lower conductivity HS bound σ_{HS-}^{-1} and is a function of the individual constituent fractions f_i and conductivities σ_i.

$$R_{HS+}^{-1} = \sigma_{HS-} = \sigma_{\min} + A_- / (1 - \alpha_- A_-) \tag{B1}$$

where

$$A_- = \sum_{i=2}^{N} f_i \Big/ [(\sigma_i - \sigma_{min})^{-1} + \alpha_-]$$

$$\alpha_- = (3\sigma_{\min})^{-1}$$

and where $\sigma_{\min} = \sigma_1$ is the minimum conductivity ($\sigma_{\min} \le \sigma_i$) and N is the total number of constituents. The lower HS bound on resistivity R_{HS-} is equal to the inverse of the upper conductivity HS bound σ_{HS+}^{-1} and is

$$R_{HS-}^{-1} = \sigma_{HS+} = \sigma_{\max} + A_+ / (1 - \alpha_+ A_+) \tag{B2}$$

where

$$A_+ = \sum_{i=1}^{N-1} f_i \Big/ [(\sigma_i - \sigma_{max})^{-1} + \alpha_+]$$

$$\alpha_+ = (3\sigma_{\max})^{-1}$$

The liquid component typically has the maximum conductivity where $\sigma_i \le \sigma_{\max} = \sigma_N$. Both the upper and lower HS bounds satisfy the conditions that the resistivity R_{HS} equals the mineral resistivity R_m when the fluid fraction is zero ($\phi = 0$) and equals the fluid resistivity R_w when the mineral fraction is zero ($\phi = 1$) (Figure B1).

The upper HS resistivity bound corresponds to isolated conductive spheres (pores) covered by a resistive shell (mineral) (Mendelson and Cohen, 1982), a likely scenario for pumice and some basalts, but an unlikely one for granular materials. The lower HS resistivity bound corresponds to isolated resistive spheres (mineral) covered by a conductive shell (water and/or clay), a more likely model for sediments. This is schematically shown in Figure B1; the black regions represent the resistive constituent and the white region the conductive constituent. Notice that both the upper and lower HS bounds are approximately linear for porosities less than approximately 0.30.

The HS bounds can be used to determine a range in the fluid volume fraction ϕ for a given R/R_w or vice versa. Other bounding models exist, however the HS bounds provide the tightest bounds for an isotropic composite without specifying the geometries of the constituents. As seen in Figure B1, the bounds are very wide for constituents with extremely different conductivities (i.e. quartz sand – fluid system) and tight for constituents with very similar conductivities (i.e. clay – fluid system). The upper bound is insignificantly influenced by the fluid resistivity $R_w = \sigma_{max}$. The lower HS bound is essentially unaffected by the mineral resistivity $R_m = \sigma_{min}$ for $\phi > 0.01$ as long as R_m/R_w is approximately greater than 10^3. In fact, Berryman (1995) showed that the lower HS bound can be simplified as a function of the fluid resistivity R_w and volume fraction ϕ in systems of insulating spherical grains saturated by a conductive fluid.

$$\frac{R_{HS-}}{R_w} \approx \frac{3-\phi}{2\phi} = \frac{3}{2}\phi^{-1} - \frac{1}{2} \tag{B3}$$

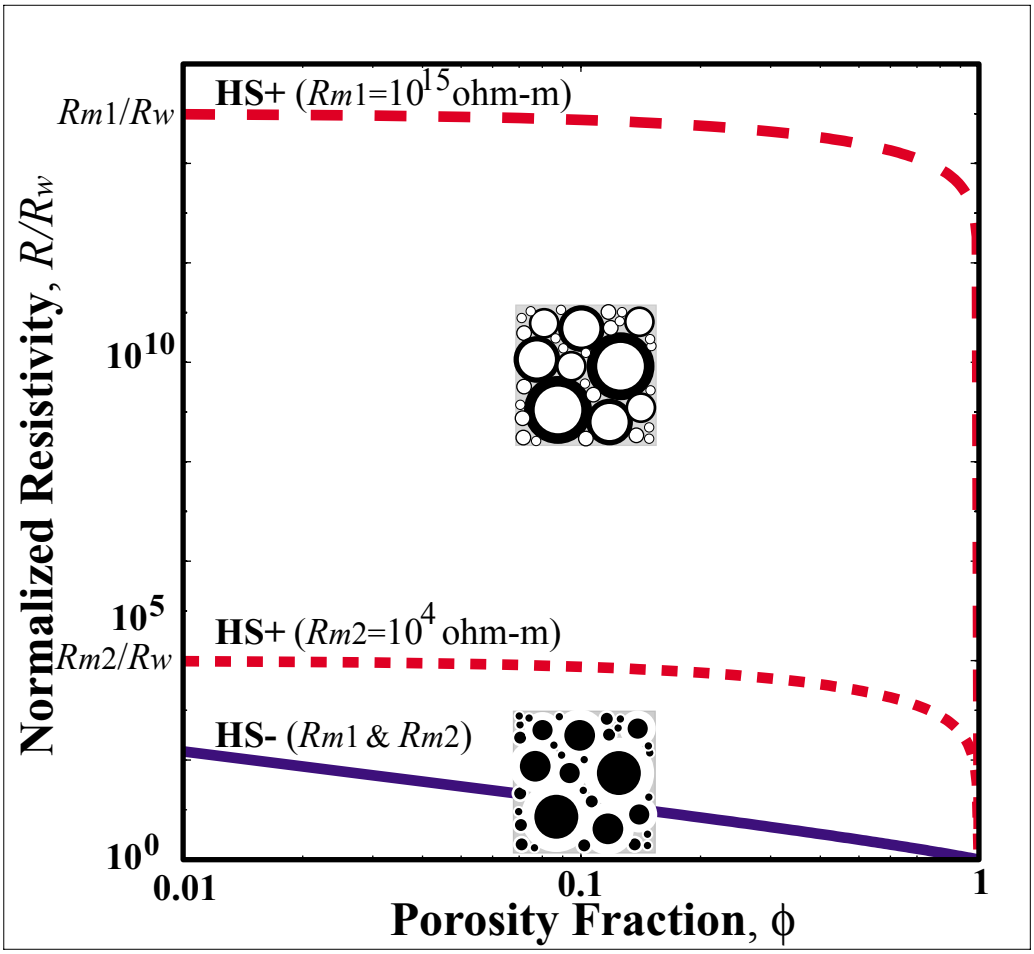

Figure B1: The Hashin- Shtrikman resistivity bounds. Example is for two systems saturated by a fluid with $R_w = \sigma_1^{-1} = 1$ Ω-m: $R_{m1} = \sigma_2^{-1} = 10^{15}$ Ω-m (dashed line) and $R_{m2} = \sigma_2^{-1} = 10^4$ Ω-m (short dashed line); the lower HS bound (bold solid line) is essentially the same at $\phi \geq 0.01$ for both systems. The black regions in the schematic sphere pack represent the resistive constituent and the white represents the conductive constituent.

Maxwell-Garnett Approximation

Maxwell (Bergman, 1978) derived a non-self-consistent theory for a system of suspended spheres, also known as the Maxwell-Garnett, Clausius-Mossotti and Lorenz-Lorentz equation. Fricke (1924) generalized the Maxwell-Garnett equation for dispersive systems spheroids. The theory describes the effective electrical conductivity σ_F^* as a function of the host volume fraction f_1, the inclusion shape parameter x, and the conductivity of the host σ_1 and of the spheroidal inclusions σ_2.

$$\frac{\sigma_F^*/\sigma_2 - 1}{\sigma_F^*/\sigma_2 + x} = f_1 \frac{\sigma_2/\sigma_1 - 1}{\sigma_2/\sigma_1 + x} \tag{B4}$$

The inclusion shape parameter x is a function of the conductivity ratio σ_2/σ_1 and the aspect ratio α (or the depolarizing factors, L_i). The equations for x are given in Fricke (1924). When modeling a sediment or rock, the host is the fluid constituent and the inclusion is the granular constituent. However, since the MG theory describes systems of spheroids in suspension, it does not necessarily hold for systems where grains are in contact. In a system of resistive spheroidal inclusions ($\sigma_2 \approx 0$) suspended in a conductive fluid, the effective resistivity R_F increases as grain ellipticity.

$$\frac{R_F}{R_w} \approx \frac{(x+1)-\phi}{x\phi} = 1 + a_F \frac{1-\phi}{\phi} = a_F \phi^{-1} + (1 - a_F) \tag{B5}$$

where

$$a_F = (x+1)/x \tag{B6}$$

In a system of resistive inclusions, x is only a function of the aspect ratio α since $\sigma_2/\sigma_1 = 0$. Fricke (1924) showed that $x = 2$ for resistive spheres, $x \approx 1.39$ for high-sphericity sands, $x \approx 0.85$ for more angular sands (Figure B2), and approaches zero for penny-shaped resistive grains. Assuming that the maximum grain eccentricity is 0.95, Mendelson and Cohen (1982) showed that in a 2-D system of aligned grains the maximum a_H is approximately 10, which corresponds to $x \approx 0.095$.

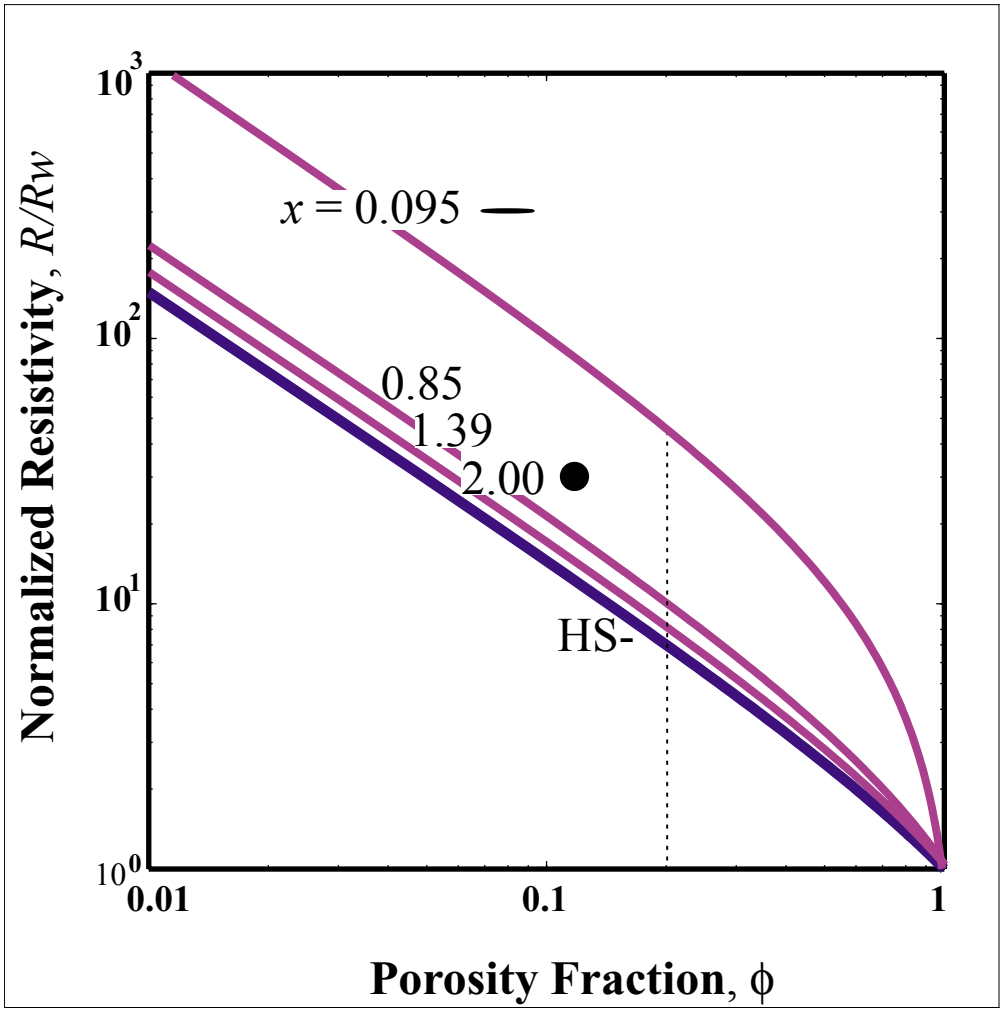

Figure B2: Modified Maxwell-Garnett approximation for resistive grains with different shapes. Example is for a system of minerals with $R_m = \sigma_2^{-1} = 10^{15}$ Ω-m and fluid with $R_w = \sigma_1^{-1} = 1$ Ω-m. The bold line for spheres ($x = 2$) corresponds to the lower HS bound. $x \approx 1.39$ in highly spherical sand grains, $x \approx 0.85$ in more angular sand grains, and $x_{max} \approx 0.095$ for platy grains. For $\phi < 0.2$, the ϕ - R/R_w relationship is nearly linear and m ≈ 1.5 and a_H increases with decreasing ellipticity. Schematic grain shapes are not to scale.

For a system of resistive grains suspended in a conducting fluid, like Eqn. B5, the effective resistivity R_F of the composite is a function of the fluid's resistivity, not of the mineral resistivity. For the specific case of a system of insulating spherical grains ($x = 2$), Eqn. B8 reduces to the lower HS bound (Eqn. B5); in other words, the minimum R_F occurs when the grains are spherical. The less spherical the grains, the further the MG curve plots above the lower HS bound. Notice, however, that for approximately $\phi < 0.20$,

m ≈ 1.5 and a_H increases as ellipticity decreases (Figure B2); in other words there is a nearly linear relationship between ϕ and R/R_w for $\phi < 0.20$ and a_H and m are independent.

Self-consistent Approximation

The self-consistent estimate of effective conductivity σ^*_{SC} for an isotropic system of ellipsoidal inclusions is a function of the inclusion depolarizing factors L_j, conductivity σ_i and volume fractions f_i (Berryman, 1995)

$$\sum_{i=1}^{N} f_i(\sigma_i - \sigma^*_{SC})P^{*i} = 0 \qquad \text{(B7)}$$

$$P^{mi} = \frac{1}{9}\sum_{j=1}^{3}\frac{1}{L_j\sigma_i + (1-L_j)\sigma_m}$$

where N is the number of constituents and L_j is defined in Appendix A. σ^*_{SC} is solved for through iteration and always satisfies the HS bounds.

SC theory describes a system where the pore space has defined inclusion shapes, unlike the MG theory. Because the pore space has a defined shape, there is a porosity limit below which the pore inclusions are no longer connected and the effective conductivity approaches zero; this porosity limit is known as the porosity percolation threshold ϕ_p. The percolation threshold is a function of pore shape in Eqn. B7; spherical pores having the largest ϕ_p and needles having the smallest ϕ_p. In a system of spherical grains and pores of different shapes, the porosity percolation threshold ϕ_p (Figure B3) is 1/3 for spherical pores (α=1), 1/5 for disk-shaped pores (α = -∞), and 0 for needle-shaped pores ($\alpha = \infty$) (Norris et al, 1985).

According to SC theory, pore and grain ellipticity have opposing effects on R; R increases from increasing pore ellipticity and decreasing grain ellipticity. SC theory predicts that resistivity data converge at $\phi \approx 0.70$ (Figure B2), regardless of the pore shape or constituent resistivities in two-constituent systems. For $\phi > 0.70$, resistivity data falls along a single curve, which is approximately equal to the lower HS bound. For $\phi <$ 0.70, the SC resistivity estimate is greatest for spherical pores and least for disk-shaped pores (Figure B2). This is likely a consequence of ellipsoid surface area; spheres have a minimum surface area per unit volume, therefore less area in contact with other pores.

The percolation threshold in natural sediments and rocks is very low, therefore the pore space likely becomes more needle-shaped as porosity decreases.

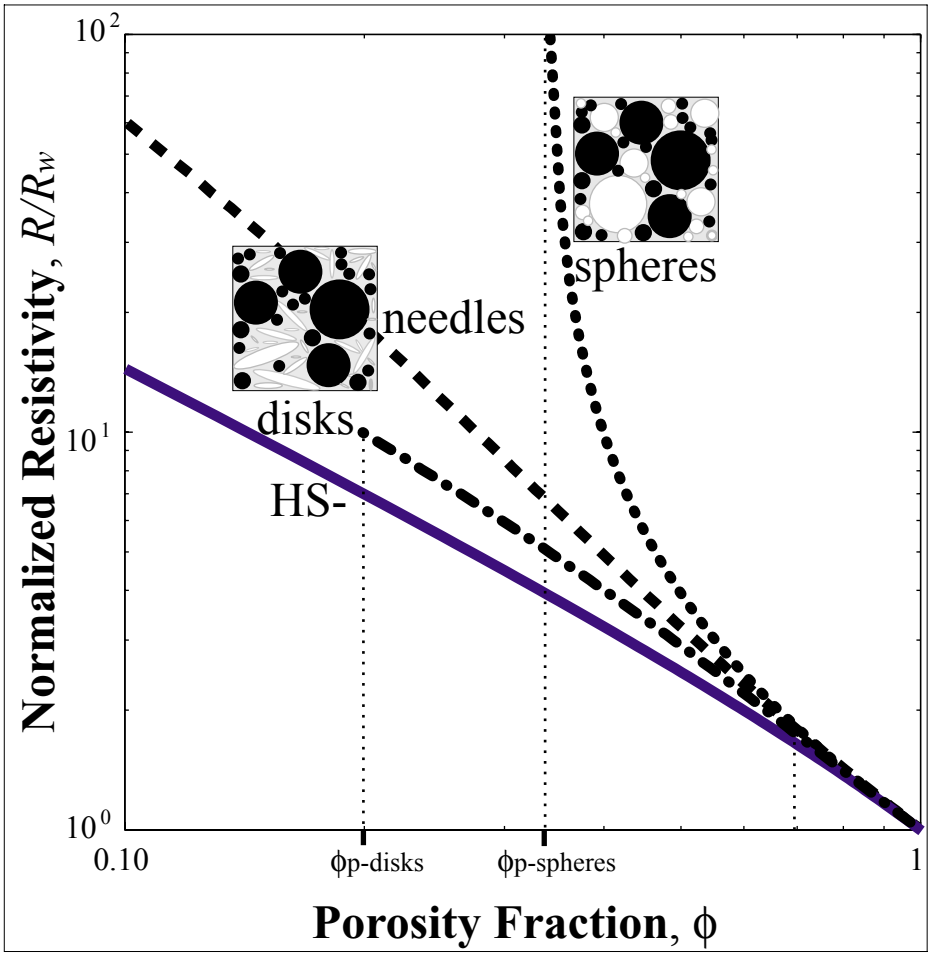

Figure B3: Self-consistent approximation for three pore shapes. Self-consistent approximations for spherical grains ($R_m = \sigma_2^{-1} = 10^{15}$ Ω-m) and pores that are spherical (dotted line), needle-shaped (dash-dot line), and disk-shaped (dashed line) ($R_w = \sigma_1^{-1} = 1$ Ω-m). The lower HS bound (bold solid line) is shown for reference. The porosity percolation threshold ϕ_p is 1/3 for spheres, 1/5 for disks, and 0 for needles. The SC curves converge at $\phi \approx 0.70$. The black regions in the schematic sphere pack represent the resistive grain constituent and the white represents the conductive pore constituent. Schematic grain shapes are not to scale.

Empirical Resistivity Background

The $R - F$ Relationship

Archie (1942) found empirically that the true resistivity R of a fully brine-saturated system of insulating grains increased linearly with varying brine resistivity R_w.

$$R = FR_w \tag{B8}$$

The proportionality constant that relates the material's true resistivity and brine resistivity is the formation resistivity factor F ($F \geq 1$).

The electrical current solely flows through the conducting liquid in a system of insulating grains with both resistive fluid (i.e. gas) and conducting liquid in the pore space (i.e. brine). In such a system, the ability for the current to flow is strongly influenced by the conducting liquid fraction S_w. Archie's water saturation equation (Archie, 1942)

$$R = FR_w S_w^{-n}, \tag{B9}$$

is a general form of Eqn. B8 that accounts for partial saturation. The saturation exponent n is approximately two (Tiab and Donaldson, 1996). The water saturation equation is typically used to predict brine saturation in systems of insulating grains, such as clean sands.

The effects of clays on R have been studied since the 1950's, however a practical and universal method for accounting for the affect of clay conductivity and particle shape still has not been developed. Two different concepts have been developed to estimate the influences of clays on R (summarized in Worthington, 1985): one is based on the clay volume fraction and the other on ionic double-layer phenomenon. Models based on the clay volume fraction are have little physical basis, however, those based on ionic double-layer phenomenon require destructive core analysis, making them less practical. Both types of models have the general form of

$$R = FR_w + X \tag{B10}$$

In clean sands, X approaches zero and Eqn. B10 reduces to Archie's equation (Eqn. B8). X is typically written either as a function of the cation exchange capacity or the distribution of clays, the clay conductivity and volume. The presence of clays leads to a non-linear relationship between R and R_w if R_w is high (Worthington, 1985). The clay

conductivity effect is insignificant in a fully brine saturated system when the ratio of the liquid to clay resistivities R_w/R_{cl} is less than 0.10 (Hoyer and Spann, 1975). Interestingly, like the theoretical Eqns. B3 and B5, the clay-adjusted models are functions of the conductive constituents, not the resistive constituents.

An example of a practical resistivity model based on the clay volume fraction is (Schlumberger, 1989)

$$R = FR_w(1-V_{cl})S_w^{-n} + \frac{R_{cl}}{V_{cl}}S_w^{-n+1} \tag{B11}$$

Eqn. B11 (same as Eqn. 2.4) is typically used to predict brine saturation in clay-rich systems, where R and R_w are measured, the clay volume fraction V_{cl} is estimated, the clay resistivity R_{cl} is assumed, and F is estimated using Eqn. B12. A variety of clay-adjusted equations have been developed that satisfy Eqn. B8 (Summarized in Worthington, 1985, Tiab and Donaldson, 1996, and Schlumberger, 1989). However, Eqn. B11 works well (Schlumberger, 1989) for many clay-rich formations, independent of the distribution of the clays (dispersed, laminated or structural). When the clay fraction is zero, Eqn. B11 reduces to Archie's water saturation equation for clean sands (Eqn. B8).

The $F - \phi$ Relationship

Much like hydraulic permeability, the formation resistivity factor F is the characteristic flow property of a material; it is a measure of the inability for an electrical current to flow through pore space. Archie derived the empirical relationship $F = \phi^{-m}$, which Winsauer et al (1952) later generalized as

$$F = \frac{a_H}{\phi^m} \tag{B12}$$

The Humble equation (Eqn. B12) is only valid for the formation's porosity range. Since the Humble equation is empirical, it is not required to meet the limiting conditions $R = R_m$ at $\phi = 0$ nor $R = R_w$ at $\phi = 1$. There isn't a percolation threshold term in the Humble equation, therefore the pore space is assumed connected for all porosities (Webman et al, 1976, 1977; Straley, 1978). Sen et al (1979) suggested modifying the Humble equation to account for the percolation threshold by

$$F = \frac{a_H}{(\phi - \phi_p)^m} \tag{B13}$$

The modification of the porosity term by subtracting the percolation threshold is similar to the modification in the Kozeny-Carman equation for permeability by Mavko and Nur (1997). The percolation threshold term in Eqn. B13 significantly influences high F values, corresponding low ϕ values; therefore a_H and m values derived from Eqn. B13 would be significantly influenced by the percolation term in low porosity data.

Eqn. B12 was derived based upon the observation of ϕ - F data for a particular formation plotting linearly on a log-log plot. For example, taking the log of both sides of Eqn. B12 leads to

$$\ln(F) = \ln(a_H) - m\ln(\phi) \tag{B14}$$

The internal geometry parameter a_H and cementation exponent m are computed as the y-intercept and negative slope, respectively, of the least-squares fit to ϕ- F data on a log-log plot (Figure B4a). a_H and m define the formation's characteristic properties therefore are computed for individual formations. a_H and m cannot be defined uniquely for a formation if either there are too few porosity data available or the porosity range is too narrow (Figure B4b), a common problem encountered with environmental data sets. In such cases, a_H and m can be extrapolated from similar hydrogeologic formations. The uncertainty in the parameters a_H and m, which define the linear relationship, can significantly influence porosity estimates that are outside the range of the porosity data.

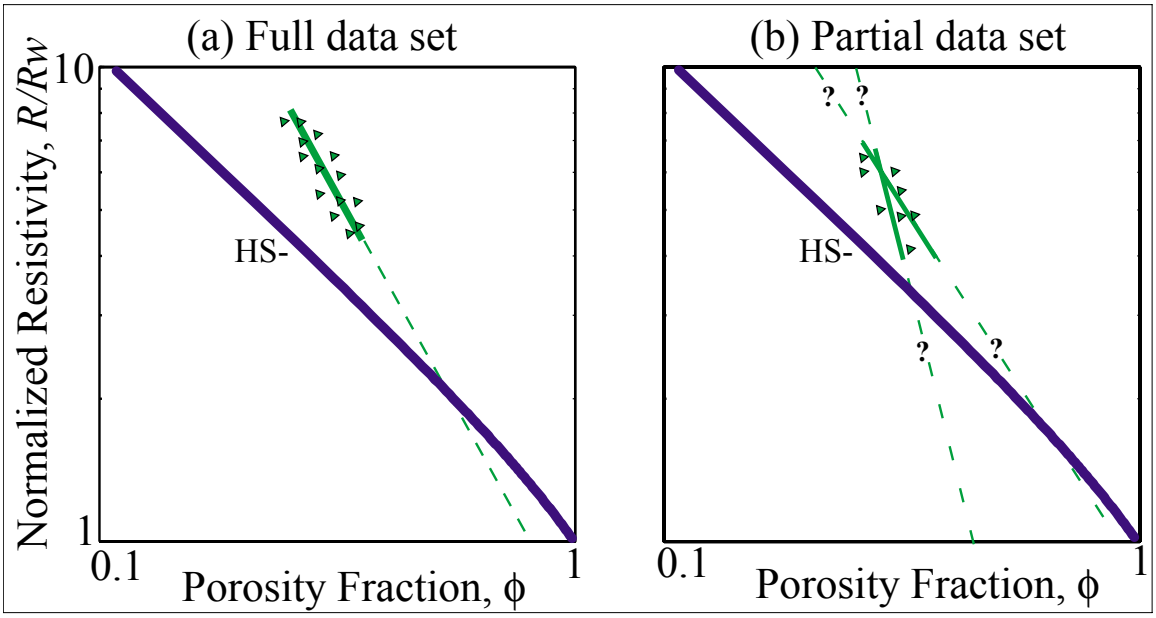

Figure B4: Linear relationship between F and ϕ on log-log plot. Example of: (a) full data set where there is a linear relationship and (b) partial data set where there is greater uncertainty in a_H and m.

Both a_H and m are to some degree influenced by pore space and bulk characteristics such as shape, sorting, packing, pore configuration and size, tortuosity, type of pore system (intergranular, intercrystalline, vuggy, fractured), compaction and clay content (Tiab and Donladson, 1996). Gomez-Rivero (1976) derived relationships between a_H and m of the form

$$\ln(a_H) = C_1 + C_2 m \tag{B15}$$

where C_1 and C_2 values for various materials are listed in Table B2. The relationship between m and $\ln(a_H)$ originates from the way a_H and m are derived in Eqn. B14. Archie (1942), on the other hand, showed that a ≈ 1 and m increases with increased cement in clean sands (Figure B5.a), and MG theory suggests that for $\phi < 0.20$, m ≈ 1.5 and a_H increases as ellipticity decreases (Figure B5.b); both suggest that a_H and m are independent since one is assumed constant. These observations suggest that if either a_H or m can be constrained then the other can be determined; this is especially significant when the porosity data range is too narrow to define a_H and m uniquely.

ID	Formation Description	y-intercept C_1	slope C_2

1	Sandstones	1.04	-0.60
2	Sands	1.40	-0.78
3	Carbonate rocks	2.26	-1.11

Table B2: Slopes and intercepts that define the $\ln(a_H) - m$ relationship for various materials (Gomez-Rivero, 1976).

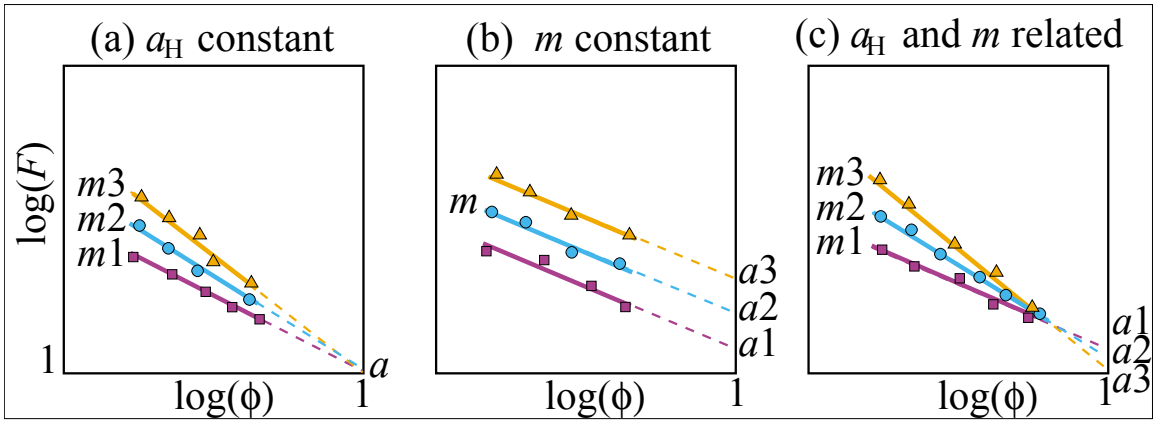

Figure B5: Schematic of a_H and m. (a) a_H constant, (b) m constant, and (c) $a_H - m$ related.

The cementation exponent m value is dominated by the presence of cement. m is much larger in cemented materials than in uncemented ones (Wyllie and Gregory, 1953), however, it has not been correlated with the amount of cement. Various authors (Neustaedter, 1968; Gomez-Rivero, 1976; Sethi, 1979) have shown correlations between m and ϕ in rocks. Perez-Rosales (1982) suggested that m is the conversion exponent between channel porosity and total porosity $\phi_{ch} = \phi^m$; the greater the m, the lesser the channel porosity ϕ_{ch} and the greater the trapped porosity ϕ_{tr}. The observed range of m is 1.2 - 4 (Mendelson and Cohen, 1982)

The internal geometry parameter a_H value appears to be dominated by the influence of tortuosity (Wyllie and Gardner, 1958; Herrick, 1988). In most natural composites, a_H doesn't vary much (Schlumberger, 1989). However, as seen in Figure B2, a_H is expected to increase significantly as grain ellipticity decreases. The theoretical range of a_H defined by grain ellipticity is 0.25 – 10 (Mendelson and Cohen, 1982).

New Results on the Resistivity – Porosity Relationship

New Insight into the Influence of Clay on R, F, a_H and m

It is standard practice to use resistivity data to solve for F using Eqn. B8 so that $F - \phi$ relationships can be determined for each formation using Eqn. B12. However, Eqn. B8 is only valid for systems of fully saturated insulating grains; it is not valid for systems of neither partial saturation nor conducting minerals ($F \neq R/R_w$). Therefore, F values published as R/R_w *do not* describe the material's flow characteristics unless in a clay-free and fully saturated systems. Solving for F correctly is particularly important when using F to solve for permeability. For this reason, R/R_w is referred to as the *normalized resistivity* throughout the rest of this section, rather than formation factor.

To better understand the difference between the normalized resistivity R/R_w and formation factor F, consider the following: electrical conductivity is analogous to hydraulic conductivity and formation resistivity factor is analogous to permeability. R/R_w is a function of F and they are only equivalent when $S_w = 1$ and $\sigma_m \approx 0$ (Eqn. B11). We suggest that it is more appropriate to solve for F using a clay-adjusted equation like Eqn. B11, rather than Eqn. B8, in systems of insulating grains with partial saturation and/or conducting minerals. Solving for F in such a way would "remove" the influence of the conducting minerals so that F would be a function of the pore space, not of the conducting mineral component.

It is important to understand the influence of clays on R and F when interpreting pore space characteristics using ϕ - R/R_w data and when comparing a_H and m values. Dispersed or structural clay can be added to a system by either replacing pore or granular volumes. The clay influences on F and R depend on the clay distribution and conductivity. Replacing pore space with clay increases F, however, effect of replacing granular volume with clay depends on the clay distribution and compaction; replacing granular volume with structural clay likely has a minimal influence on F and replacing the same granular volume with dispersed clay likely increases F and the degree of influence depends on the clay compaction. There are two competing effects of clays on R; (1) the conductivity effect: the high conductivity of clays decreases the bulk mineral

resistivity, which contributes to a decrease in R, and (2) the tortuosity effect of dispersed clays: the presence of dispersed clays increases F, which contributes to an increase in R.

The influences of clay on F are shown in Figure B6.a. Replacing pore space with platy dispersed clays significantly increases F by increasing tortuosity and trapped porosity. This effect is theoretically described by Eqn. B4 (Figure B2) and empirically accounted for in the internal geometry parameter a_H, a measure of tortuosity (Eqn. B12). However, if the same amount of pore space is replaced with structural clays (i.e. shale fragments), then the influence of clay on F is minimal since the tortuosity wouldn't change significantly; it is essentially a sorting effect. Therefore, the slope $-m$ on a log-log ϕ - F plot should be greater for systems of dispersed clays than for systems of structural clays (Figure B6.a).

The influences of replacing sand pore space with clay on resistivity are summarized in Table B3 and schematically shown in Figure B6.b. The influences of clay on R depend on the clay's conductivity, volume and distribution within the sand's pore space (Eqn. B11). The clay conductivity effect is insignificant in a fully brine saturated system when the ratio of the liquid to clay resistivities R_w/R_{cl} is less than 0.10 (Hoyer and Spann, 1975). In such systems, the influence of clay is solely through tortuosity, therefore the influence on R/R_w is the same as on F (Figures B6.a and B6.b). In a saturated freshwater system, the clay tortuosity effect likely dominates when dispersed clay fills the pore space, resulting in a high R, whereas the clay conductivity effect likely dominates when structural clays fill the same amount of pore space, resulting in low R (Figure B6.b).

Erickson and Jarrard (1998) used ϕ - R/R_w data in high porosity, clay rich materials to show that muds have higher m and lower a_H values than clay-rich sands. The data they used also shows a transition in the ϕ - R/R_w relationship between clay-rich sands and sandy muds at $\phi \approx 0.55$, which is approximately the critical porosity of sand; in other words, like work by Marion (1990), the critical porosity defines the transition between clay-dominated and sand-dominated systems. In the sand-dominated system, dispersed clays replace pore space and in the clay-dominated system, dispersed clays essentially replace sand grains. Several other authors (Carothers, 1968; Porter and Carothers, 1971) have observed that ϕ - R/R_w data in clay-rich sands typically have low m and unusually high a_H values, whereas ϕ - R/R_w data in muds and shales have high m and low a_H values

(Schlumberger, 1989). The unusually high a_H values in clay-rich sands are likely either a consequence of the non-linear dependence of R on clay volume (Eqn. B11) or a grain shape effect; according to MG theory, R is higher for platy grains than spherical ones.

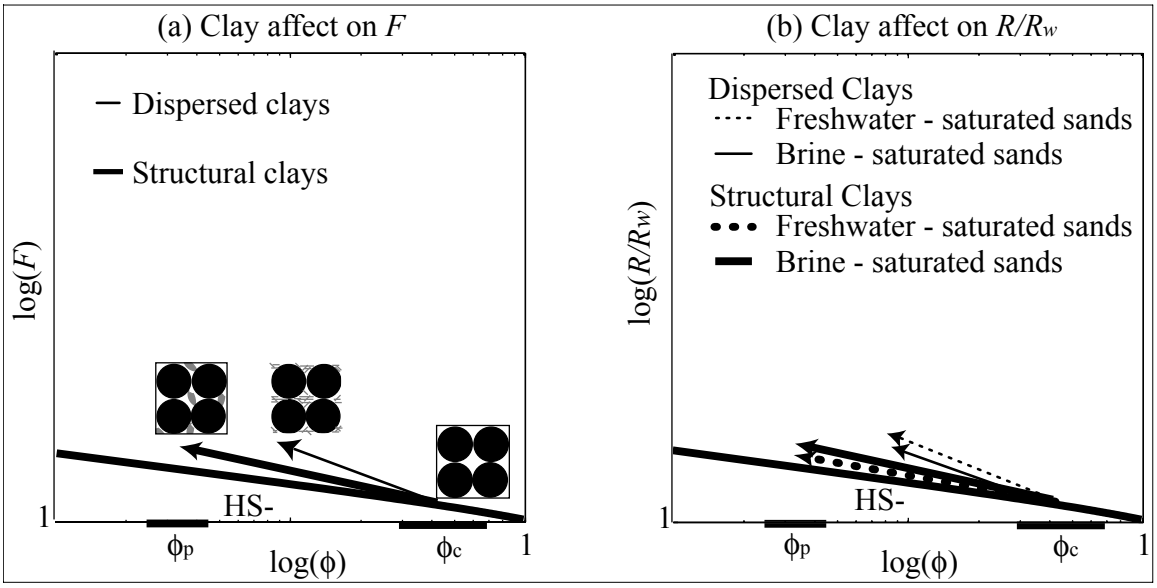

Figure B6: The influence of clays on F and R. The influence of adding clay to a sand system: (a) the influence on F of adding dispersed and structural clays to a saturated sand and (b) the influence on R/R_w of adding dispersed and structural clays to brine and freshwater saturated sands.

Adding clay to sand pore space	Conductivity effect	Tortuosity effect
dispersed clays to brine saturated sands	insignificant	increases
dispersed clays to freshwater sands	decreases	increases
structural clays to brine saturated sands	insignificant	slightly increases
structural clays to freshwater sands	decreases	slightly increases

Table B3: The proposed influence of dispersed and structural clays in freshwater and brine-saturated sands on resistivity.

Evaluating Pore Space Characteristics using ϕ - R/R_w Data

Changes within a formation can occur from the addition or subtraction of material from the pore or granular volumes. When the granular volume changes, the resistivity might change without a change in porosity, such as replacing resistive sand grains with shale fragments or spherical grains with elliptical ones. However, when the pore volume changes there is a change in both resistivity and porosity. Changes in a composite's pore space characteristics can occur from changes in cementation, compaction, sorting, grain ellipticity and clay volume. Trends of data on an ϕ - R/R_w plot can help identify the varying pore space characteristics within a particular formation and delineate individual formations with different characteristic properties.

R/R_w increases from increased tortuosity and trapped porosity; this occurs from changes in the pore space characteristics such as increased clay volume, cementation (Archie, 1942) and compaction (Tiab and Donaldson, 1996) and decreased sorting (large grain size distribution) (Wyllie and Gregory, 1953) and granular ellipticity (Fricke, 1924) in a system. These same changes in pore space characteristics result in a reduction of the system's total porosity ϕ (Wyllie and Gregory, 1953; Maxwell, 1960; Beard and Weyl, 1973).

The location of data on a ϕ - R/R_w plot can be thought of as a particular stage of evolution in the complexity of a simple system's pore space. For example, let's say the original system is of well-sorted, single constituent, loosely-packed grains and for simplicity of explanation, assume the grains are resistive and spherical (Figures B7 a, b and c). In such a system, ϕ - R/R_w data plot at the system's origin, which is defined by the point on the lower HS bound evaluated at the system's critical porosity ϕ_c (Figures B7 a, b and c); the lower HS bound coincides with the MG curve for suspended spherical grains. As the system's ϕ decreases from a particular pore space property, R/R_w increases linearly on a log-log plot, resulting in a fan of lines emanating from the system's origin. The slope $-m$ and y-intercept $\ln(a_H)$ of the line depends on the pore space property that is changing. For example, increasing the degree of cementation has a more significant affect on R/R_w than ϕ, therefore m is high and a_H is low (Figure B7.b). Decreasing the sorting of the sphere pack has a lesser effect than cementation on R/R_w at the same porosity, therefore m is lower and a_H is higher (Figure B7.a). As the loose spheres

become compacted (Figure B7.c), they are arranged into tighter packing, increasing R/R_w and decreasing ϕ.

If instead of spherical grains, the original system is of aspherical, well-sorted, single constituent, loosely-packed, resistive grains, then the system's origin is defined by the point on the MG curve (Eqn. B4; dashed line in Figures B7 d, e and f) evaluated at the system's critical porosity ϕ_c. For grains of low sphericity, the MG curve plots above the lower HS bound (Figure B2) and the system's critical porosity is greater than that of spheres. As explained by MG theory, increased grain ellipticity in grain-supported systems insignificantly influences m, however increases a_H, so the slopes are approximately the same as in Figures B7 a, b and c.

In most natural systems, a combination of pore space properties can influence the system's ϕ_c, which could result in linear trends that don't precisely intersect the original system's origin. However as seen in Figure B8, for the most part, the hypothesis of lines converging near the lower HS bound at the critical porosities of granular systems is a good approximation in a wide variety of systems. This hypothesis suggests that as m increases, $\ln(a_H)$ decreases linearly, and the linear relationship between m and $\ln(a_H)$ is defined by the system's origin. The relationship between a_H and m is discussed below.

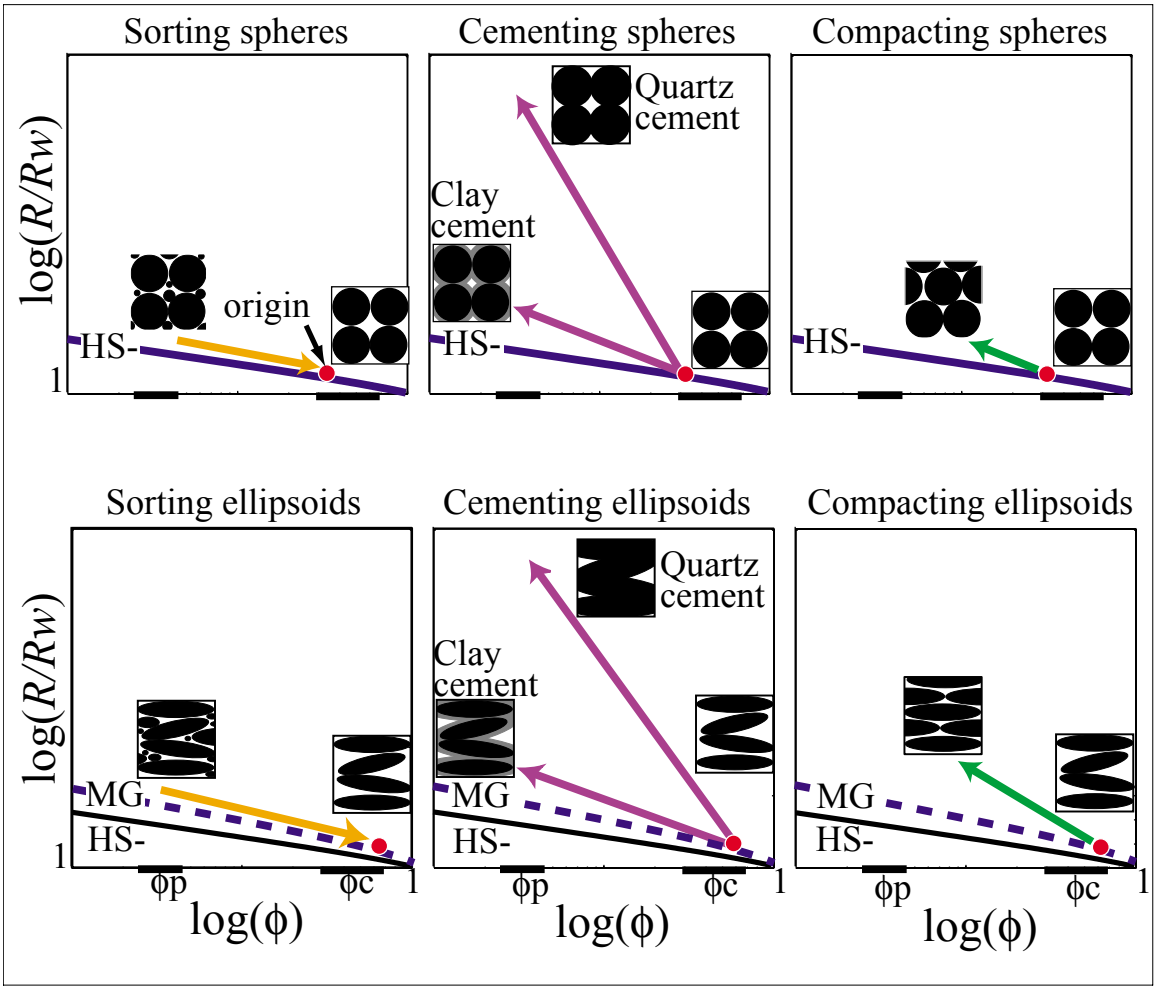

Figure B7: Schematic of the influence of ellipticity, sorting, cement and compaction on F and ϕ. The influence of (a,d) sorting, (b,e) cement and (c,f) compaction on F and ϕ in systems of spherical and aspherical grains. The arrows indicate direction of increased change in property. The bold solid line is the lower HS bound (Eqn. B2.1) and the bold dashed line in is the MG curve for elliptical grains (Eqn. B5).

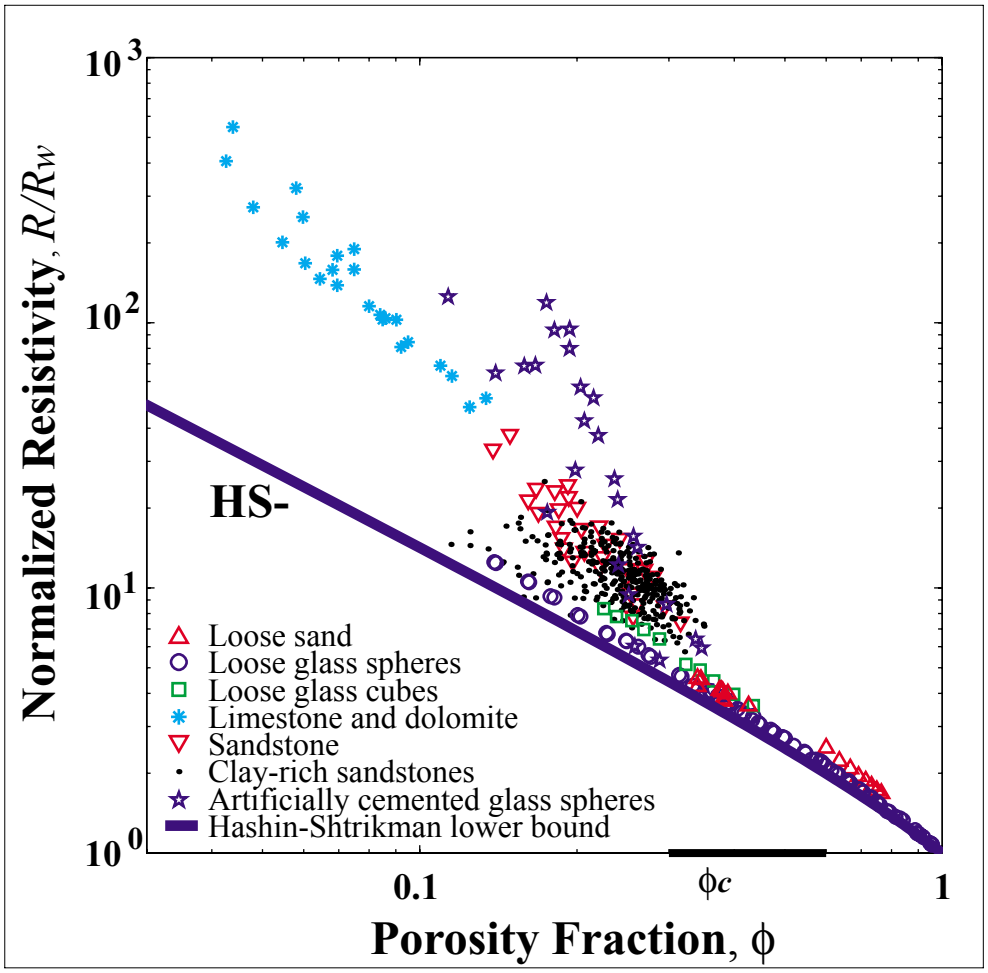

Figure B8: R/R_w - ϕ lab and field data. Shown are: loose clean sands (Wyllie and Gregory, 1953; Fricke, 1924), loose glass spheres (Wyllie and Gregory, 1953; Klinkenberg, 1951; Slawinski, 1926; Balderas-Joers, 1975), loose glass cubes (Wyllie and Gregory, 1953), limestones and dolomites (Mendoza-Romero and Perez-Rosales, 1985), sandstone (Winsauer et al, 1952; Wyllie and Spangler, 1952; Sanyal et al, 1973; Wyllie and Rose, 1950), clay-rich sandstone (Porter and Carothers, 1971), and artificially cemented glass spheres (Wyllie and Gregory, 1953); the lower HS bound (solid line) is plotted for reference. Data converges near the HS lower bound at approximately $0.30 \leq \phi \leq 0.4$.

New a_H - m Relationship

Both a_H and m are, to some degree, influenced by the same pore space and bulk characteristics and are likely related. And, as seen in Figure B8, ϕ - R/R_w data converge towards the lower HS bound evaluated at porosities near the critical porosities of granular systems. This suggests that as m increases, $\ln(a_H)$ decreases linearly, and the linear relationship between m and $\ln(a_H)$ is defined by critical porosity and grain shape. The

point defined by the MG curve for the primary constituent's shape evaluated at the composite's critical porosity (ϕ_c, R^*_{MG}/R_w) may be a pivot point for linear R/R_w – ϕ relationships (Figures B7 and B6.c). By solving for ln(a) in Eqn. B14 and substituting Eqn. B5 in for F evaluated at ϕ_c gives

$$\ln(a_H) = C_1 + C_2 m \tag{B16}$$

where

$$C_1 = ln(\frac{(x+1)-\phi_c}{x\phi_c}) = ln(\frac{a_F}{\phi_c} + 1 - a_F) \tag{B17}$$

$$C_2 = \ln(\phi_c - \phi_p) \tag{B18}$$

Eqn. B16 is of the same form as the empirical relationship derived by Gomez-Rivero (1976), where the y-intercept C_1 and slope C_2 are the formation-specific constants in Eqn. B15 and Table B2. The ϕ_c and x values in Table B4 were found by solving for ϕ_c in Eqn. B18 and x in Eqn. B17 in terms of the empirically derived C_1 and C_2 values in Table B2. These ϕ_c and x values represent the overall values for each formation represented by an a_H – m data pair. As discussed earlier and defined by Eqn. B5, for each formation, the MG curve corresponding to x evaluated at ϕ_c defines the origin from which linear ϕ - F relationships emanate (Figure B9).

ID	Formation	calculated ϕ_c	published ϕ_c	calculated x	published x
1	Sandstones	0.33	0.40 [(1)]	0.83	--
2	Sands	0.46	--	0.63	0.85 [(2)]
3	Carbonate rocks	0.55	0.60 [(1)]	0.31	--

Table B4: Calculated ϕ_c and x values from C_1 and C_2 values by Gomez-Rivero (1976) in found in Table B1; published ϕ_c and x values (1) Mavko et al (1998) & (2) Fricke (1924).

The ϕ_c and x values found using Eqns. B17 and B18 agree very well with published values (Table B2) even though Gomez-Rivero's empirical relationships were derived from $F = R/R_w$ data in partially brine-saturated, clay-rich materials. Eqns. B16 – B18 are particularly useful when the porosity data range is too narrow to define a_H and m uniquely and either a_H and m can be estimated.

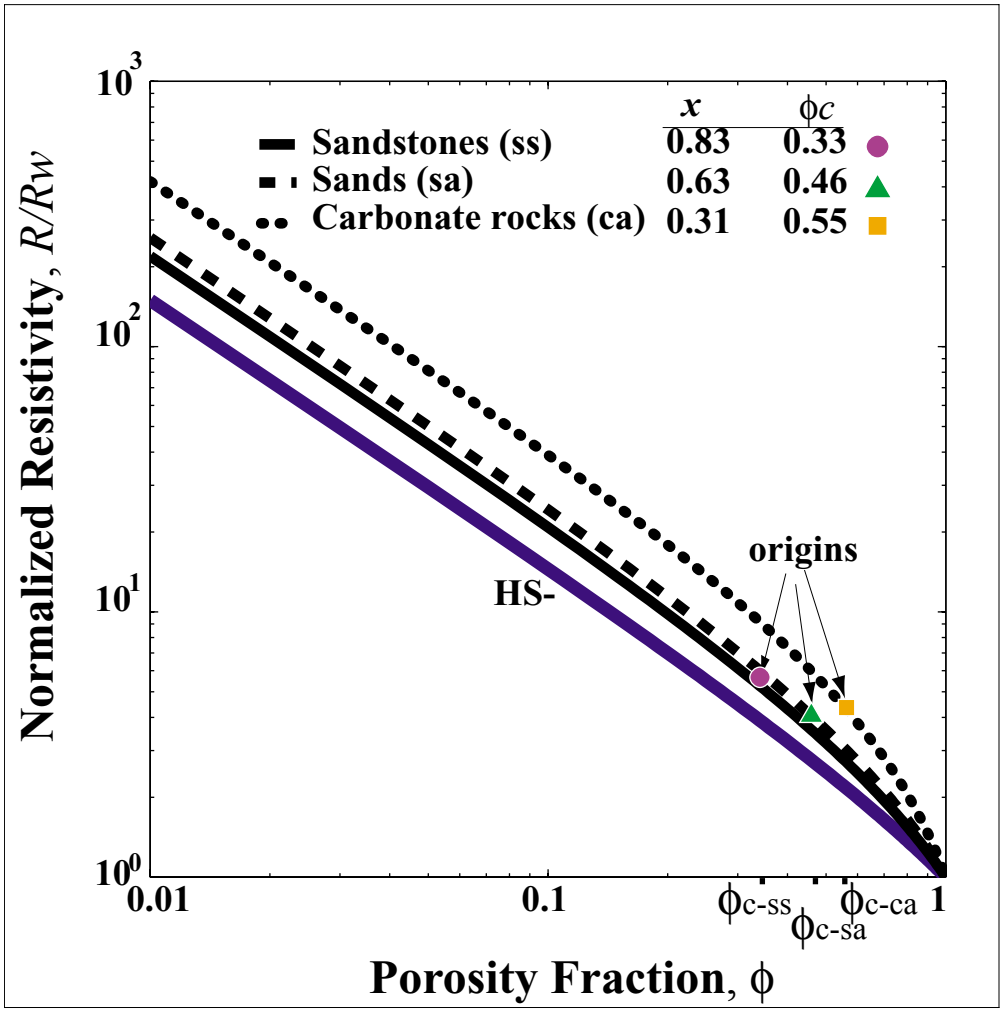

Figure B9: The pivot points of linear $R/R_w - \phi$ relationships. The x and ϕ_c values determined from $a_H - m$ relationships for different formations define the pivot points (origins) for linear $R/R_w - \phi$ relationships.

Defining a Generalized Archie's Equation

As discussed in above, a formation's total and channel porosities are related by a normalizing factor A (Eqn. A11), which is a function of the critical porosity, percolation threshold, and Archie's exponent m. The A factor is essentially adsorbed into the formation-specific, empirical constant a_H in the Humble equation (Eqn. B12). a_H can be expressed in terms of A by solving for a_H in Eqns. B16 – B18 and assuming a porosity term of the form $(\phi - \phi_p)^m$ in Eqn. B13.

$$a_H = \frac{a_F}{A} + \frac{(1-a_F)}{A}\phi_c = \frac{x+1-\phi_c}{Ax} \tag{B19}$$

Eqn. B19 is useful for estimating a_H when too few porosity measurements are available to define a linear relationship between ϕ and R/R_w. From Eqns. B13 and B19, a general Archie's equation can be expressed in terms of a system's channel porosity, grain shape parameter, and critical porosity by

$$F = \frac{x+1-\phi_c}{x\phi_{ch}} \tag{B20}$$

Eqn. 20 is particularly useful for determining F when channel porosity is measured.

The ϕ - R/R_w Relationship Re-defined in Three Porosity Regions

At very low porosities, there exists a porosity limit, known as the percolation threshold ϕ_p, below which the pore space is no longer connected and the electrical resistivity approaches the mineral resistivity. Also, at porosities between 0.30 and 0.40, the range in critical porosities ϕ_c of sands and sphere packs (Wyllie and Gregory, 1953; Mavko et al, 1998), resistivity values in cemented and uncemented sands and glass spheres converge near the lower HS bound (Figure B8). The critical porosity and percolation threshold define three porosity regions in which the $F - \phi$ relationship is defined (Table B3 and Figure B10). Region I is defined for $\phi < \phi_p$ where the pore space is no longer connected ($\phi_{ch} = 0$) and the resistivity theoretically approaches the bulk mineral resistivity value; this region may be approximated by the upper HS bound (Eqn. B2), however we have not come across published data in this low porosity region. Region II is defined for $\phi_p \le \phi \le \phi_c$ where resistivity and porosity are linearly related on a log-log plot and where the pore space is connected but not all is available for flow (trapped porosity ϕ_{tr} exists). This region, where most data in sediments and rocks fall (Figure B8), can be modeled well by the Humble equation (Eqn. B12) and is bounded by the lower HS bound and an empirical upper bound F_+. Region III is defined for $\phi > \phi_c$ where the mineral constituents are suspended and all of the pore space is available for flow ($\phi_{tr} = 0$); resistivity in this region is approximated by the lower HS bound (Figures B1, B3 and B8).

For $\phi_p < \phi < \phi_c$, we suggest that ϕ - R/R_w data converge at ϕ_c because ϕ_{tr} decreases and ϕ_{ch} increases as ϕ increases within this porosity region, making it easier for electrical currents to flow through the pore space. At $\phi > \phi_c$, we suggest that ϕ - R/R_w data fall along a single curve because all of the pore space is available for flow ($m = 1$, so $\phi_{ch} = \phi$) and the tortuosity is low ($a_H \approx 1$) in this porosity region.

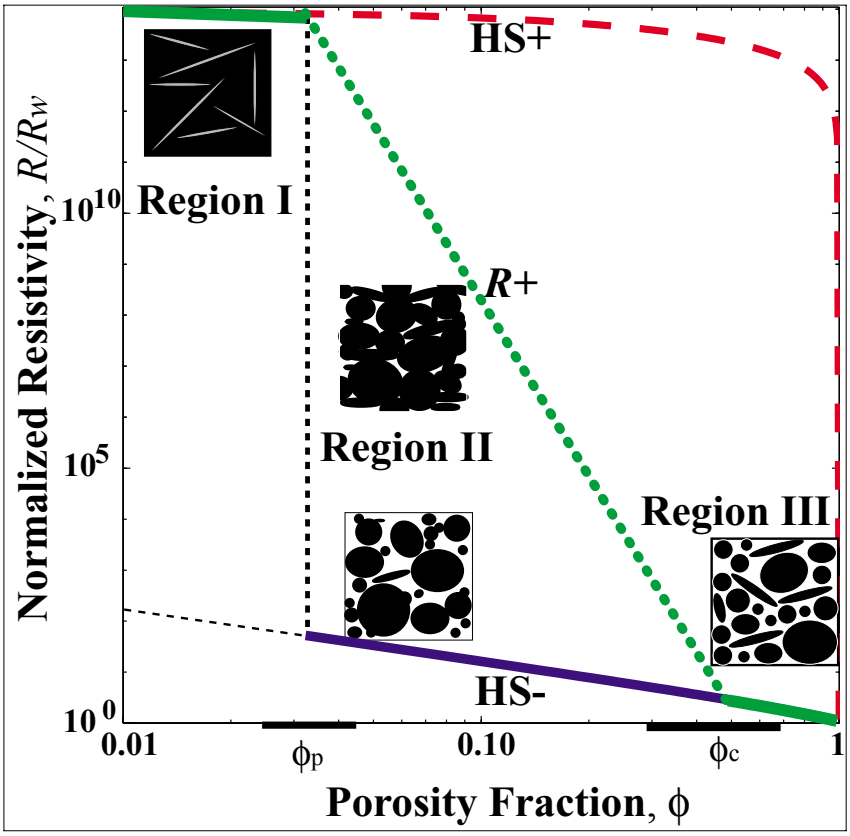

Figure B10: Three regions of the ϕ - R/R_w relationship defined by the percolation threshold ϕ_p and critical porosity ϕ_c. The ϕ - R/R_w relationship is defined by (1) the upper HS bound for $\phi < \phi_p$, (2) the Humble equation for $\phi_p \le \phi \le \phi_c$, and (3) the lower HS bound for $\phi > \phi_c$.

Region	Porosity Range	Total Porosity	Channel Porosity	Normalized Resistivity
I	$0 < \phi < \phi_p$	$\phi = \phi_{tr}$	$\phi_{ch} = 0$	R_{HS+}/R_w (Eqn. 2)
II	$\phi_p \le \phi \le \phi_c$	$\phi = \phi_{ch} + \phi_{tr}$	$\phi_{ch} = A(\phi - \phi_p)^m$	$a_H / (\phi - \phi_p)^n$ (Eqn. B13)
III	$\phi_c < \phi \le 1$	$\phi = \phi_{ch}$	$\phi_{ch} = \phi$	R_{HS-}/R_w (Eqn. 1)

Table B3: Regions of the ϕ - R/R_w relationship defined by the percolation threshold ϕ_p and critical porosity ϕ_c.

New Upper ϕ - R/R_w Bound

The upper HS bound immediately approaches the bulk mineral constituent resistivity at the onset of adding resistive minerals to a fluid (Figure B10). This behavior is not observed in granular media; in fact, data in granular media do not plot near the upper HS bound regardless of the pore space characteristics. Perhaps, this is because the upper HS bound represents isolated conductive spheres covered by a resistive shell (Figure B1), a valid scenario in few rocks (i.e. basalts where the pore space is defined by trapped air bubbles). It is an unlikely scenario in sediments where the resistive grains make up the ellipsoidal component of the system. The upper HS bound therefore is of limited use in sediments and most rocks.

We define an empirical upper bound R_+ that is lower than the upper HS bound and is defined by a line that connects the points (ϕ_p, R^*_{HS+}/R_w) and (ϕ_c, R^*_{HS-}/R_w) on a log-log plot. The first point corresponds to the upper HS bound evaluated at the percolation threshold ϕ_p; the second point corresponds to the lower HS bound evaluated at the critical porosity ϕ_c. This idea stems from work done by Nur et al (1995) on modifying the upper bound for the acoustic velocity – porosity relationship. This linear upper bound corresponds to the Humble equation (Eqn. B12), where

$$\frac{R_+}{R_w} = \frac{a_+}{(\phi - \phi_p)^{m_+}} \tag{B21}$$

where $\phi_p \le \phi \le \phi_c$ and

$$m_+ = \frac{\ln\left(R^*_{HS+}/R^*_{HS-}\right)}{\ln\left(\phi_c/\phi_p\right)} \tag{B22}$$

$$a_+ = exp[ln(R^*_{HS-}/R_w) + m_+ ln(\phi_c - \phi_p)] \tag{B23}$$

The empirical upper bound and lower HS bound are narrow for porosities near ϕ_c and wide for porosities near ϕ_p (Figure B10). ϕ - R/R_w data in unconsolidated glass sphere packs fall just above the lower HS bound for $\phi < \phi_c$ and on the lower HS bound for $\phi > \phi_c$ (Figures B8 and B11). Data in artificially cemented glass spheres plot just below the empirical upper ϕ - R/R_w bound (Figure B11).

The maximum a_+ is 1.5, the a_H of the lower bound for $\phi < \phi_c$, since one end member is defined by the lower HS bound. Small variations in ϕ_p and ϕ_c significantly influence the log intercept a_+ and slightly influence the slope $-m$ of the empirical upper bound. For example, for $R_m = 10^{14}$ Ω-m and $R_w = 1$ Ω-m, $\phi_p = 0.035 \pm 0.01$ (28% uncertainty) and $\phi_c = 0.40 \pm 0.05$ (28% uncertainty) leads to $a_+ = 2.75 \cdot 10^{-5} \pm 2.31 \cdot 10^{-4}$ (843% uncertainty) and $m_+ = 12.75 \pm 0.73$ (5.7% uncertainty). The uncertainty of a_+ is statistically very significant because of the log dependence of a_H, however, as seen in Figure B10, it has nominal influence on the upper bound on a log-log plot.

A modified upper HS bound R_{MHS+} (Figure B11) can be defined by evaluating the upper HS bound for $\phi^* = \phi/\phi_c$, where $0 \le \phi^* \le 1$ and $0 \le \phi \le \phi_c$ and the end members are defined by (0, R_m/R_w) and (ϕ_c, R^*_{HS-}/R_w). However, like the upper HS bound, the modified upper HS bound immediately approaches the mineral resistivity at the onset of adding the resistive mineral constituent to the fluid constituent. As shown in Figure B11, data do not plot near the modified upper HS bound, regardless of the pore space characteristics.

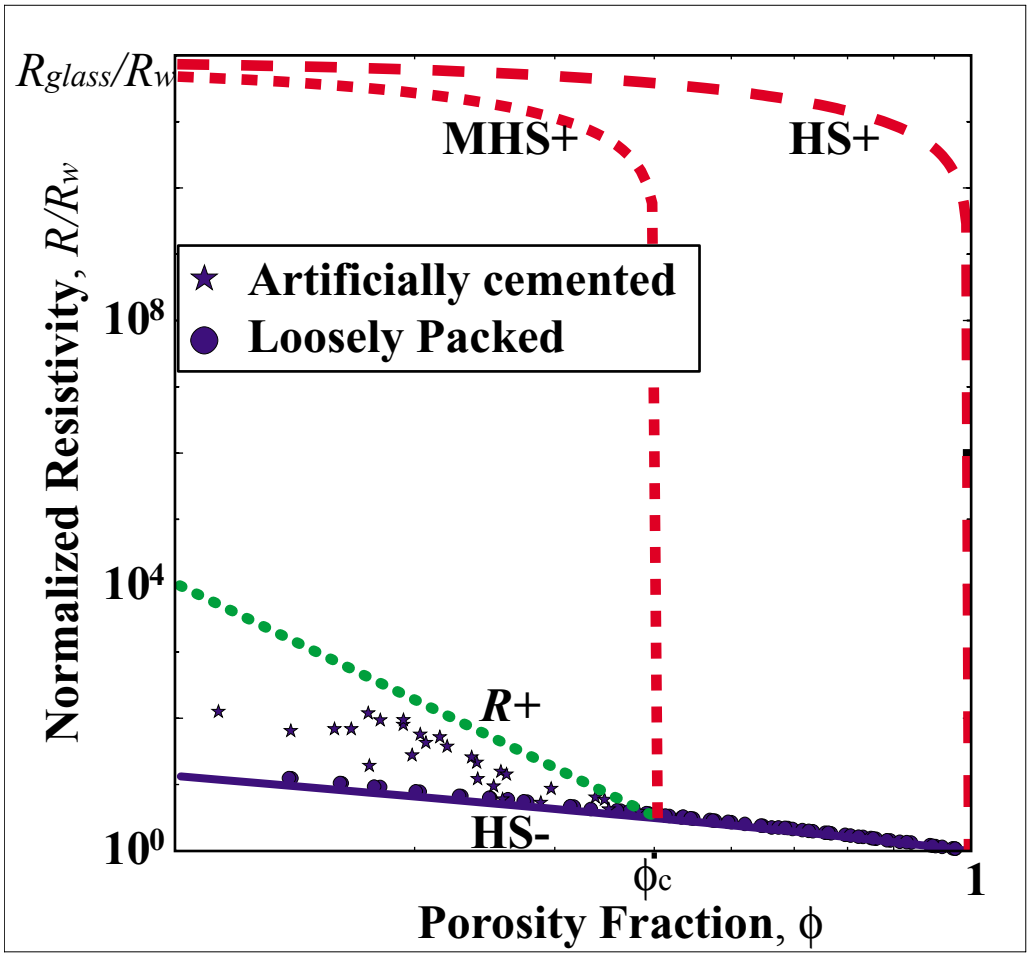

Figure B11: The empirical upper ϕ - R/R_w bound. R/R_w – ϕ lab data for loose glass spheres (circles) and artificially cemented glass spheres (stars) from Wyllie and Gregory (1953); the HS bounds (solid and dashed lines), the modified upper HS bound (short dashed line), and the empirical upper bound (dotted line), where $\phi_c = 0.40$, $\phi_p = 0.035$, $R_m = 10^{14}$ Ω - m and $R_w = 1$ Ω - m. Data is also plotted in Figure B8.

Conclusions

- F values published as $F = R/R_w$ do not describe the material's flow characteristics unless in a clay-free and fully saturated systems.

- Increasing clay content increases F, however there are two competing effects on R: (1) the conductivity effect: the high conductivity of clays decreases the bulk mineral resistivity (Eqn. B8), which contributes to a decrease in R, and (2) the tortuosity effect: the presence of dispersed clays increases F, which contributes to an increase in R.

- The lower Hashin-Shtrikman bound is independent of the mineral resistivities and volume fractions if R_m/R_w is greater than approximately 10^3.

- In systems of resistive and conductive constituents, it is the conductive constituent's resistivity and volume, not the resistive constituent's resistivity and volume, that define the behavior of the lower HS bound, the MG equation, and the empirical relationships.

- In a given formation, the formation resistivity factor may increase and porosity may decrease from an increase in clay content, compaction, or cementation or a decrease in grain ellipticity or sorting; the data trends (a_H and m) on a $F - \phi$ plot can help diagnose the property causing the change.

- According to MG theory, grain ellipticity influences a_H significantly and m insignificantly in grain-supported unconsolidated composites ($\phi < 0.20$).

- Adding clay to the pore space of a sand system will result in an increased formation factor and decreased porosity, regardless of the clay structure; however, depending on the clay structure and the ratio R_{cl}/R_w, it will result in either an increase or decrease in the measured resistivity.

- $F - \phi$ data in unconsolidated glass sphere packs fall just above the lower HS bound for $\phi < \phi_c$ and on the lower HS bound for $\phi > \phi_c$.

- The HS bounds and MG theory are approximately linear for $\phi < 0.20$.

- SC theory predicts that resistivity converges at $\phi \approx 0.70$, regardless of the pore shape and constituent resistivity in a two-component system.

- The ϕ R/R_w data in sands and sphere packs tend to converge near the lower HS bound at porosities between approximately 0.30 and 0.40, which correspond to the critical porosities of sands and spheres.

- The ϕ - R/R_w relationship can be defined by three regions: (1) for $\phi \leq \phi_p$, $R/R_w \approx R_{HS+}/R_w$, (2) for $\phi_p < \phi < \phi_c$, $R/R_w = a/\phi^m$, and (3) for $\phi \geq \phi_c$, $R/R_w \approx R_{HS-}/R_w$.

- For $\phi_p < \phi < \phi_c$, ϕ - R/R_w data converge at the critical porosity because ϕ_{tr} decreases and ϕ_{ch} increases as ϕ increases within this porosity region.

- At $\phi > \phi_c$, ϕ - R/R_w data fall along a single curve because all of the pore space is available for flow ($m = 1$, so $\phi_{ch} = \phi$) and the tortuosity is low ($a_H \approx 1$) in this porosity region.

- An empirical upper bound on the R/R_w relationship can be defined by the line $F_+ = a_+ / \phi^{m_+}$, where a_+ and m_+ are the *y*-intercept and negative slope of a line that connects the points (ϕ_p, R^*_{HS+}/R_w) and (ϕ_c, R^*_{HS-}/R_w) on a log-log plot.

- The $a_H - m$ relationship can be expressed as a function of the primary constituent's critical porosity and grain shape.

References

Archie, G.E., 1942. The electrical resistivity log as an aid in determining some reservoir characteristics. *Trans. Am. Inst. Mech. Eng.,* 146, 54-62.

Balderas-Joers, C., 1975. Estudio experimental del factor de resistivitidad y la porosidad en medios no consolidados de muy alta porosidad. Tesis profesional, Universidad Nacional Autonoma de Mexico.

Beard, D.C. and Weyl, P.K., 1973. Influence of texture on porosity and permeability of unconsolidated sand. *Bull., AAPG*, 57, 2, 349 – 369.

Bergman, D.J., 1978. The dielectric constant of a composite material – a problem in classical physics. *Phys. Reports*, 43, 377 – 407.

Berryman, J. G., 1995. Mixture theories for rock properties, in *Rock Physics and Phase Relations: A Handbook of Physical Constants*. T. J. Ahrens, ed., American Geophysical Union, Washington, D. C., 205-228.

Carothers, J.E., 1968. A statistical study of the formation factor relation. *The Log Analyst*, IX, Sept. – Oct.

Fricke, H., 1924. A mathematical treatment of the electric conductivity and capacity of disperse systems. *Phys. Rev*., 24, 575 – 587.

Gal, D., Dvorkin, J., and Nur, A., 1998. A physical model for the porosity reduction in sandstones. *Geophys*., 63, 454 – 459.

Gomez-Rivero, O., 1976. A practical method for determining cementation exponents and some other parameters as an aid in well log analysis. *The Log Analyst*, 27, 8 – 24.

Gueguen, Y., and Palciauskas V., 1994. *Introduction to the Physics of Rocks*. Princeton University Press, Princeton.

Herrick, D.C., 1988. Conductivity models, pore geometry, and conduction mechanisms. Ann. *SPWLA, 29th Ann. Log. Symp*., June, Paper D, 1-17.

Hashin, Z., and Shtrikman, S., 1962. A variational approach to the theory of effective magnetic permeability of multiphase materials. *J. Appl. Phys.*, 33, 3125-3131.

Hoyer, W.A. and Spann, M.M., 1975. Comments on obtaining accurate electrical properties of cores. *Trans. SPWLA XVI.*

Klinkenberg, L.J., 1951. Analogy between diffusion and electrical conductivity in porous rocks. *Bull., GSA*, 62, 559 – 563.

Marion, D.P., 1990, Acoustical, Mechanical, and Transport Properties of Sediments and Granular Materials, Ph.D. thesis, Stanford University.

Mavko, G., and Nur, A., 1997. The effect of a percolation threshold in the Kozeny-Carman relation. *Geophys*., 1480 – 1482.

Mavko, G., Mukerji, T., and Dvorkin, J., 1998, *The Rock Physics Handbook: tools for seismic analysis in porous media*, Cambrige University Press.

Maxwell, J.C., 1960. Experiments on compaction and cementation of sand. *Rock deformation – A Symposium, Boulder, CO: Geological Society of America (GSA)*. Ed. D.T. Griggs. Ch. 5, 105 – 132.

Mendelson, K.S., and Cohen, M.H., 1982. The effect of grain anisotropy on the electrical properties of sedimentary rocks. *Geophys*., 47, 257 – 263.

Mendoza-Romero, G., and Perez-Rosales, C., 1985. New relationship between formation resistivity factor and primary and secondary porosities. *SPWLA, 26th Ann. Log. Symp*., June, 1-19.

Neustaedter, R.H., 1968. Log evaluation of deep Ellenberg gas zones. Paper SPE 2071, presented at *The Deep Drilling and Development Symposium – Deleware Basin of the SPE of AIME*, Monahans, Texas, Mar. 28.

Norris, A.N., Sheng, P., and Callegari, A.J., 1984. Effective-medium theories for two-phase dielectric media. *J. Appl. Phys*., 57, 1990 – 1996.

Nur, A., Mavko, G., Dvorkin, J., and Gal, D., 1995. Critical Porosity: The key to relating physical properties to porosity in rocks, in *Proc., 65th Ann. Int. Meeting, Soc. Expl. Geophys*., 878.

Parkhomenko, E. I., 1967, *Electrical Properties of Rocks*, Plenum Press, New York.

Perez-Rosales, C., 1982, On the Relationship Between Formation Resistivity Factor and Porosity, *Soc. Pet. Eng. J.*, 531-536.

Porter, C.R., and Carothers, J.E., Formation factor – porosity relation derived from well log data. *The Log Analyst*, Jan. – Feb., 16 – 26.

Rider, M.H., 1991. *The Geological Interpretation of Well Logs*; Revised Edition. Whittles Publishing.

Sanyal, S.K., Marsden, S.S., Jr., and Ramey, H.J., Jr., 1973. *The Log Analyst*, Mar. – Apr., 10 – 24.

Schlumberger, 1989, *Log Interpretation Principles/Applications*, Schlumberger Educational Services, Houston.

Sen, P.N., Scala, C., and Cohen, M.H., 1981. A self-similar model for sedimentary rocks with application to the dielectric constant of fused glass beads. *Geophys.*, V. 46, N. 5, 781 – 795.

Sethi, D.K., 1979. Some considerations about the formation resistivity factor – porosity relations. *Transactions of the SPWLA 20th Annual Logging Symposium*, Tulsa, Paper L.

Slawinski, A., 1926. Conductivilite d'un electrolyte contentant des spheres dielectriques, *J. Chim. Phys*., 23, 710 – 727.

Tiab, D. and Donladson, E. C., 1996, Petrophysics: Theory and Practice of Measuring Reservoir Rock and Fluid Transport Properties, Gulf Publishing Co., Houston Texas.

Waxman, M.H. and Smits, L.J.M., 1968. Electrical conductivities in oil-bearing shaly sands. *Soc. Pet. Engrs. J.*, 9, 107 – 122.

Winsauer, W.O., Shearin, H.M. Jr., Masson, P.H., and Williams, M., 1952. Resistivity of Brine-Saturated Sands in Relation to Pore Geometry. *Bull., AAPG*, 36, 2, 253-277.

Worthington, P.F., 1985. Evolution of shaley sand concepts in reservoir evaluation. *The Log Analyst*, 26, 23-40.

Wyllie, M.R.J., and Gardner, G.H.F, 1958. The generalized Koseny-Carman equation. *World Oil*, Mar.

Wyllie, M.R.J., and Gregory, A.R., 1953. Formation factors of unconsolidated porous media: Influence of particle shape and effect of cementation. *Trans. Am. Inst. Mech. Eng*., 198, 103-110.

Wyllie, M.R.J., and Rose, W.D., Some theoretical considerations related to the quantitative evaluation of the physical characteristics of reservoir rock from electrical log data. *Trans., AIME*, 189, 105 – 118.

Wyllie, M.R.J., and Spangler, M.B., 1952. Application of electrical resistivity measurements to problem of fluid flow in porous media. *Bull. AAPG*, 36, 359 – 403.

C. DEVELOPMENTS IN THE ELECTRICAL RESISTIVITY – ACOUSTIC VELOCITY RELATIONSHIP

Introduction

Up until approximately 10 years ago, the use of seismic methods for environmental groundwater investigation had been nearly non-existent. The advantages of using seismic methods for delineating hydrostratigraphic units have been recently recognized by the environmental community and significant advances have been made in shallow seismic acquisition techniques and processing. Not only is the environmental community using compressional wave data more frequently, but also the geotechnical community is using surface and VSP shear wave data more frequently to study ground stability. Electrical resistivity techniques, on the other hand, have been used for decades to qualitatively interpret changes in fluid properties and locate clay-rich formations. For the most part, the environmental community *qualitatively* analyzes seismic and resistivity data *independently*.

As explained earlier, a system's percolation threshold ϕ_p and critical porosity ϕ_c together define three distinct porosity regions, within which the formation resistivity factor – channel porosity and the moduli – total porosity relationships are defined. The porosities of most natural materials fall within the second porosity region (Region II), where $\phi_p \leq \phi \leq \phi_c$. In this region, the abilities for electrical currents and acoustic waves to

be transmitted through the system are influenced by changes in various pore space characteristics, such as pore structure (amount, texture and content), grain contacts (shape, sorting and cement degree and type) and clays (amount, type and distribution). These pore space characteristics define the relationship between the channel porosity available for electrical flow and the total porosity through which a seismic wave travels. Therefore, seismic and electrical techniques can be used jointly to constrain porosity, a required parameter for fluid flow modeling.

This section focuses on theoretically and empirically exploring the relationship between electrical resistivity and seismic velocity. The most significant contributions of this work are the development of resistivity – velocity bounds and insight into determining formation pore space characteristics using resistivity – velocity data. The real significance of these results, however, is the potential for using known relationships between resistivity and material properties to explain velocity trends and vice versa. Both the petroleum and environmental industries would benefit from these results because of the potential for using electrical logs to better constrain seismic interpretations and develop more accurate maps of flow properties.

Background

Theoretical Velocity Background

Elastic Properties

The compressional and shear velocities, V_p and V_s, at which an acoustic wave travels through an isotropic, homogeneous, elastic system, are functions of the system's bulk density ρ and elastic moduli K and μ (Mavko et al, 1998).

$$V_p = \left(\frac{K + \frac{4}{3}\mu}{\rho}\right)^{\frac{1}{2}} \tag{C1}$$

$$V_s = \left(\frac{\mu}{\rho}\right)^{\frac{1}{2}} \tag{C2}$$

The system's bulk density ρ is equal to the geometric mean of the individual constituent's densities ρ_i.

$$\rho = \sum_{i=1}^{N} f_i \rho_i \tag{C3}$$

The system's effective bulk K and shear μ moduli are controlled by the system's pore space characteristics and the individual constituent's elastic properties and volume fractions. Most mineral constituents (excluding clay) are stiff and rigid, whereas clays and fluids (gas and/or liquid) are compressible (low K) and lack rigidity ($\mu = 0$) (Table C1). Because the moduli of minerals and fluids are so different, the amount of pore-filling fluid ϕ strongly influences the system's effective moduli and velocities. Changes in a system's pore space characteristics can cause changes in the constituent volume fractions and the type and number of granular contacts, thus changing the system's effective elastic moduli and density.

A system's Poisson's ratio ν is a function of the system's effective bulk and shear moduli, not of the density.

$$\nu = \frac{3K - 2\mu}{2(3K + \mu)} = \frac{V_p^2 - 2V_s^2}{2(V_p^2 - V_s^2)} \tag{C4}$$

where $-1 \leq \nu \leq 0.5$. In fluids, $\nu = 0.5$ since $\mu = 0$ GPa. Therefore, materials with Poisson's ratios near 0.5 have fluid-like behavior. ν characterizes the ability for a composite to deform horizontally when compressed vertically. Most natural composites expand horizontally (positive ν) under vertical compression, as opposed to contracting (negative ν); therefore, it is safe to assume ν is between 0 and 0.5 in rocks and sediments (Table C1). ν is high in unconsolidated systems, regardless of the mineral constituents since the grains move freely when compressed; however, in cemented systems, ν depends on the system's mineral moduli and porosity.

Constituent	K (GPa)	μ (GPa)	ρ (g/cc)	V_p (km/s)	V_s (km/s)	σ
water	2.2	0	1	1.48	0	0.5
quartz	36.5 – 37.9	44.0 – 45.6	2.65	6.04 – 6.06	4.09 – 4.15	0.06 – 0.08
calcite	63.7 – 76.8	28.4 – 32.0	2.70 – 2.71	6.26 – 6.64	3.24 – 3.44	0.29 – 0.32
clay	1.5 – 25.0	1.4 – 9.0	1.58 – 2.60	1.44 – 4.32	0.93 – 2.54	0.14 – 0.35

Table C1: Elastic moduli and density of a few common constituents. Values from Mavko et al (1998).

Hashin-Shtrikman Bounds

The Hashin-Shtrikman (HS) bounds (Hashin and Shtrikman, 1963) are the narrowest theoretical moduli - porosity bounds that don't take the geometry of each constituent into account. For a two-constituent system, the bounds on bulk $K_{HS\pm}$ and shear $\mu_{HS\pm}$ moduli are

$$K_{HS\pm} = K_1 + \frac{f_2}{(K_2 - K_1)^{-1} + f_1(K_1 + \frac{4}{3}\mu_1)^{-1}} \tag{C5}$$

$$\mu_{HS\pm} = \mu_1 + \frac{f_2}{(\mu_2 - \mu_1)^{-1} + \frac{2f_1(K_1+2\mu_1)}{5\mu_1(K_1+\frac{4}{3}\mu_1)}} \tag{C6}$$

where f is the constituent fraction (Mavko et al, 1998). In a fluid – mineral system, the fraction of the fluid is equal to the total porosity ϕ and the fraction of the mineral is (1-ϕ). The upper bounds are typically found when the mineral is the first constituent and the fluid is the second, whereas the lower bounds are typically found when the fluid is the first constituent and the mineral is the second. The velocity – porosity bounds and Poisson's ratio – porosity bounds are found by evaluating Eqns. C5 & C6 at specific porosities and plugging the results into Eqns. C1 – C4, respectively. The bounds are wide when the constituent moduli are significantly different, such as a quartz – water

system, and tight when the constituent moduli are similar, such as a clay – water system (Figure C1).

The upper HS bound corresponds to isolated soft spheres (pores) covered by a stiff and rigid shell (mineral), a likely scenario in pumice and some basalts, but an unlikely one for granular materials. The lower HS bound corresponds to isolated stiff and rigid spheres (mineral) covered by a soft shell (water and/or clay), a more likely model for sediments. This is schematically shown in Figure C1; the black regions represent the stiff constituent and the white region the compliant one. Like the resistivity lower HS bound, the elastic lower HS bounds are controlled by the fluid constituent, not the mineral constituent, therefore the lower bounds are nearly the same for clays and quartz systems.

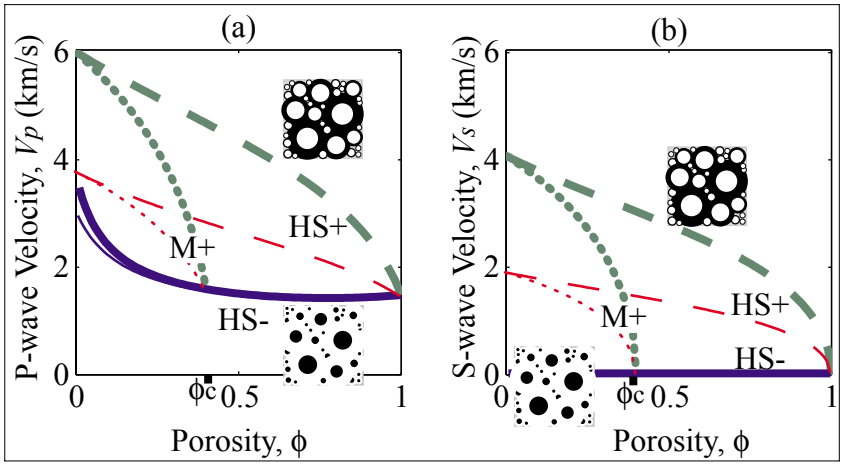

Figure C1: Upper and lower HS bounds for P-wave velocity V_p and S-wave velocity V_s. The upper (dashed lines) and lower (solid lines) HS bounds are found for two different saturated, two-constituent systems where the fluid constituent is water (K_w = 2.2 GPa, μ_w = 0 GPa, and ρ_w = 1 g/cc) and the mineral constituent is (1) quartz (K_{qz} = 37.0 GPa, μ_{qz} = 44.0 GPa, and ρ_{qz} = 2.65 g/cc) and (2) clay (K_{cl} = 25 GPa, μ_{cl} = 9 GPa, and ρ_{cl} = 2.55 g/cc). Also shown are empirical upper bounds (dotted lines) evaluated between $0 \le \phi \le \phi_c$; ϕ_c = 0.40. The black regions in the schematic packs represent the rigid and stiff constituent and the white represents the compressible and compliant one.

Empirical Velocity Background

Empirical Upper Moduli – Porosity Bounds

In granular materials, there is a critical porosity ϕ_c that separates both the mechanical and acoustical behaviors into two distinct domains (Nur et al, 1995). At $\phi < \phi_c$ the grain-supported material is rigid and stiff, whereas at $\phi > \phi_c$ the fluid-supported material is compliant and is highly compressible. Velocity – porosity data converge near the lower HS bound evaluated at the formation's ϕ_c. Nur et al (1995) defined empirical upper $K - \phi$ and $\mu - \phi$ bounds that are tighter than the upper HS bound by a line that connects the points (0, K_m) and (ϕ_c, K^*_{HS-}) and the points (0, μ_m) and (ϕ_c, μ^*_{HS-}), respectively. The first point corresponds to the mineral moduli (K_m and μ_m) when the mineral fraction is 100% ($\phi = 0$); the second point corresponds to the lower HS bound (K^*_{HS-} and μ^*_{HS-}) evaluated at the critical porosity ϕ_c. In a two-constituent fluid-mineral system, the upper moduli bounds M_+ (Mavko et al, 1998) for the bulk and shear modulus are defined by

$$M_{+} = (1 - \frac{\phi}{\phi_c}) M_m^* + \frac{\phi}{\phi_c} M_{HS-}^* \qquad \text{(C7)}$$

where M_m^* is the mineral modulus and M_{HS-}^* is the modulus of the HS lower bound evaluate at the system's critical porosity. Eqn. C7 is essentially the Voigt upper bound of the modulus for porosities normalized by the critical porosity. Empirical upper bounds on $V_p - \phi$ and $V_s - \phi$ can be created using the empirical upper K_+ and μ_+ bounds (Figures C1). Since V_p and V_s are functions of the square root of the moduli, the upper bounds aren't linear on velocity – porosity plots.

Influence of Pore Space Characteristics on P-wave Velocity and Porosity

A formation's stiffness, rigidity, density and porosity can all change from changes in pore space characteristics (i.e. cementation, compaction, sorting, clay volume, and fluid saturation). The influences of pore space characteristics on total and channel porosities are discussed later. The influences of evolution of a formation's pore space on electrical resistivity - porosity data were discussed earlier. As shown in Figure C2, the observed influences on P-wave velocity – porosity data are quite similar; i.e. sorting influences the seismic response less than cementation does. Each pore space characteristic has a different effect on porosity and elastic moduli, therefore the location of P-wave velocity – porosity data with respect to the upper and lower bounds can provide insight into the formation's pore space characteristics (Figure C2). Since V_s data is collected less commonly than V_p data, the observed influences of pore space characteristics on V_s and ν are not as well known, therefore not discussed.

$V_p - \phi$ data values of loose, unconsolidated materials tend to fall along lower HS bounds (Figure 3) as a result of changes in sorting (Avseth et al, 1998). $V_p - \phi$ data values in rock and artificially consolidated materials plot near the empirical upper bound defined by Nur (1995) as a result of increased cementation (Dvorkin and Nur, 1996). Increased compaction (Mindlin, 1949) results in increased V_p and decreased ϕ. V_p increases and ϕ decreases when dispersed clay (Han, 1986) is added to a sand matrix, whereas V_p decreases and ϕ increases when dispersed clay is added to a clay matrix (Marion, 1990). For a given formation, the velocity is higher if it is fully saturated than if it is partially

saturated; the degree of influence is controlled by the pore-filling fluid properties and the distribution, uniform (Gassmann, 1951) or patchy (Hill, 1963).

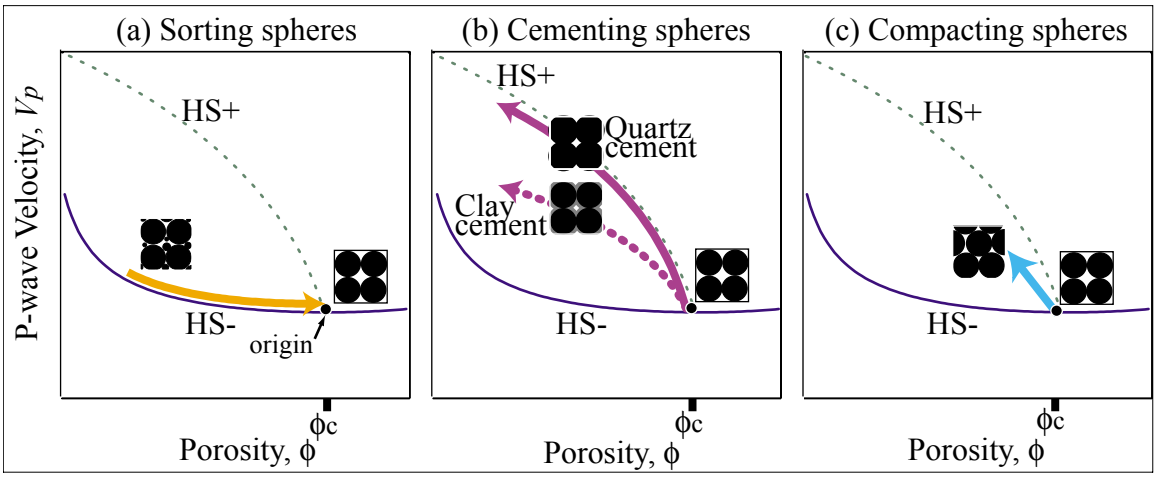

Figure C2: Schematic of the influence of pore space characteristics on V_p and ϕ. The arrows indicate direction of increased change in material property and the slopes indicate the degree of influence on V_p and ϕ. The solid lines are the upper and lower HS bounds and the dashed lines are the empirical upper bounds; $\phi_c = 0.40$.

New Developments on the Electrical Resistivity – Acoustic Velocity Relationship

New Concept of Creating Resistivity –Velocity Bounds

A formation's characteristic P-wave velocity V_p, S-wave velocity V_s, and normalized resistivity R/R_w increase with decreasing total porosity ϕ (Figures C1 a and b). For suspended granular systems ($\phi > \phi_c$), the $R/R_w - V$ relationships are all simply defined by the lower HS bounds for resistivity and moduli (Eqns. B2, C5 and C6; Figures B1 and C1). For grain-supported systems ($\phi < \phi_c$), the $R/R_w - V$ relationships are confined by upper and lower resistivity – moduli bounds (Figure C3). The $R/R_w - V_p$ bounds are created by combining the lower HS bounds (Eqns. B2, C5 and C6) and the empirical upper bounds (Eqns. B20 and C7) for R and the moduli at equal porosities. The same concept can be used to create $V_s - \phi$ bounds (Figure C3 b). The following parameters need to be specified to create the bounds: each constituent's R, K, μ, and ρ and the system's porosity limits ϕ_p and ϕ_c.

The lines in Figure C3 are example bounds for a quartz-water system. The bold solid line results from combining the lower HS R/R_w and V_p bounds; the bold dotted line results from combining the empirical upper R/R_w and V_p bounds; the dashed lines result from combining the empirical upper R/R_w bound with the lower HS V_p bound and vice versa. Strictly speaking, $R/R_w - V_p$ data can fall anywhere between the dashed lines, however, these lines correspond to the special case of a material property influencing V_p and without influencing R at a given porosity and vice versa. Values along the bounds in Figure C3 represent porosity values in 0.1 increments: from 0% porosity at the upper limit and 100% porosity at the lower limit.

A significant observation in Figure C3a is that the upper and lower $R/R_w - V_p$ bound are very similar. If the elastic and electrical properties of a formation change in a similar manner from a change in porosity, then $R/R_w - V_p$ data is restricted to the narrow region between the bounds. If an $R/R_w - V_p$ data pair plots within the region between the upper and lower $R/R_w - \phi$ bounds (solid and dotted lines in Figure C3a), then the formation

properties are electrically and elastically similar. However, if the elastic properties change without the electrical properties changing in a similar way, the $R/R_w - V_p$ data pair will plot outside the inner-most bounds, but still between the upper-lower bounds (dashed lines in Figure C3a).

The range in $R/R_w - V_p$ value pairs at a given porosity is restricted to the region defined by the box in Figure C4. The range in possible $R/R_w - V_p$ data pairs is narrow at porosities near ϕ_c since the bounds converge at ϕ_c. The $R/R_w - V_p$ data pairs are not uniquely defined for a given porosity; the range $R/R_w - V_p$ data defined by the box in Figure C4 can occur at porosities between ϕ_{min} and ϕ_{max}.

Even though an $R/R_w - V_p$ data pair plots as a single point on a $R/R_w - V_p$ plot, it is not defined uniquely by porosity; the data pair represents a range in possible porosities (Figure C5). For a given $R/R_w - V_p$ data pair, the porosity range is improved if the range limits are different for the $R - \phi$ bounds and the $V_p - \phi$ bounds.

A significant observation in Figure C5c is that the upper and lower $R/R_w - V_p$ bound are very similar. This means that the resistivity and velocity bounds have similar functional form. If the elastic and electrical properties of a formation change in a similar manner from a change in porosity, then $R/R_w - V_p$ data is restricted to the narrow region between the bounds. If an $R/R_w - V_p$ data pair plots within the region between the upper and lower $R/R_w - \phi$ bounds (solid and dotted lines in Figure C5c), then the formation properties are electrically and elastically similar. However, if the elastic properties change without the electrical properties changing in a similar way, the $R/R_w - V_p$ data pair will plot outside the inner-most bounds, but still between the upper-lower bounds (dashed lines in Figure C5c).

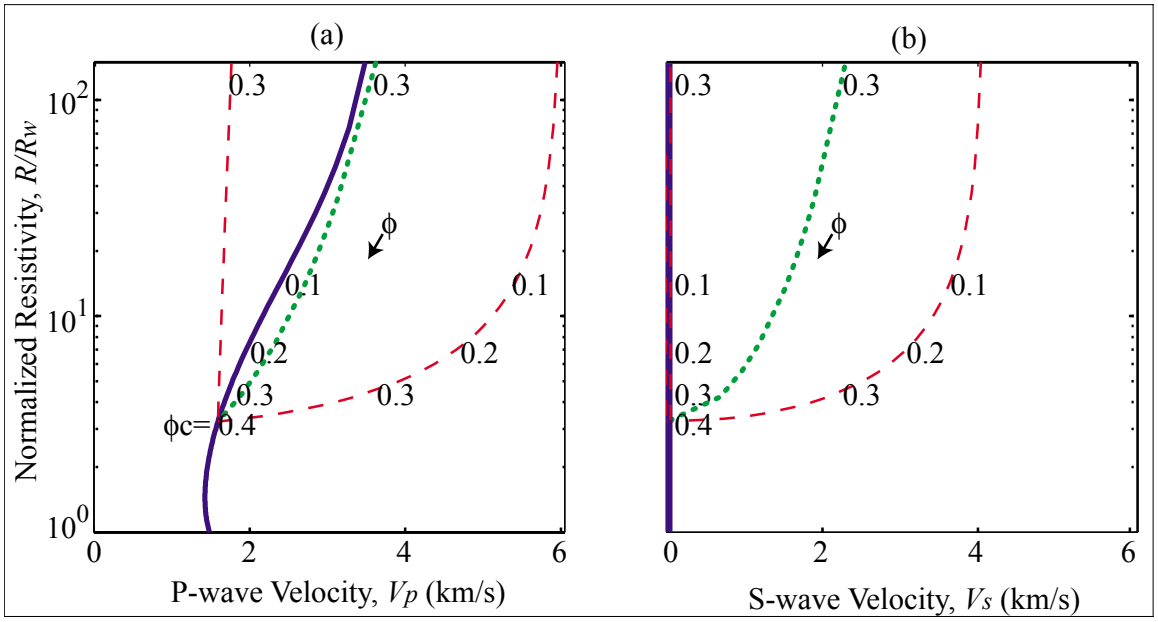

Figure C3: Bounds on the velocity – normalized resistivity. Upper and lower bounds in a water – quartz sand system for (a) V_p – R/R_w and (b) V_s – R/R_w. The lower HS bound (solid lines), the empirical upper bound (dotted lines), the upper empirical and lower HS bounds (dashed lines); ϕ_c = 0.40.

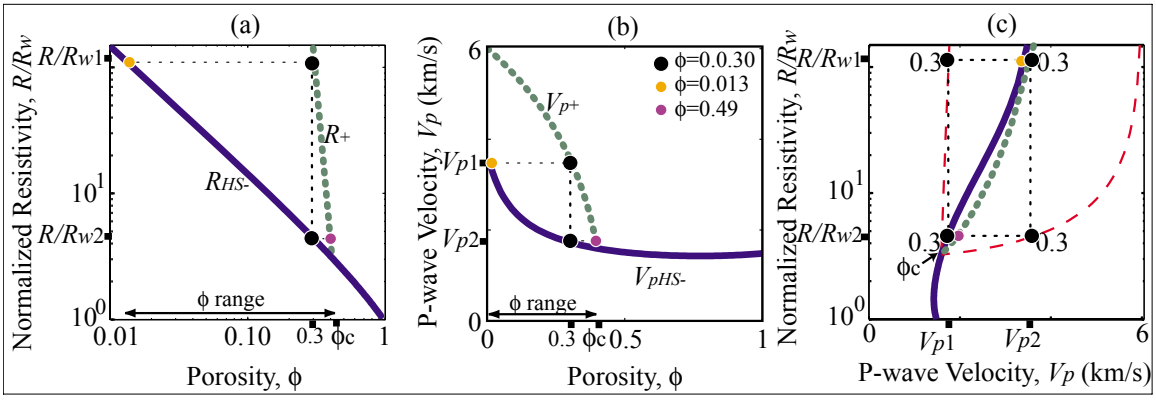

Figure C4: Constraining velocity – resistivity pairs using porosity data. Constraining porosity estimates using velocity – resistivity data. $\phi_c = 0.40$

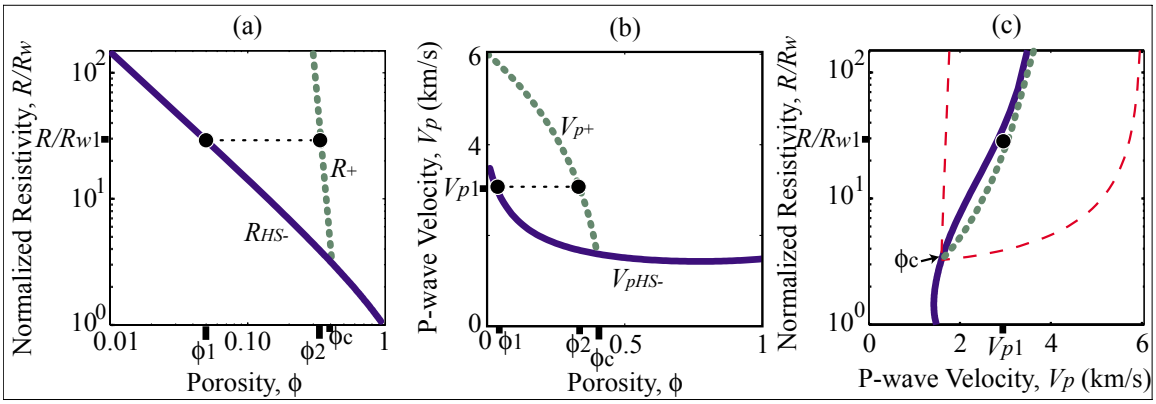

Figure C5: Constraining porosity estimates using velocity – resistivity data. $\phi_c = 0.40$

Evaluating Pore Space Characteristics using Velocity - Resistivity Data

Increasing the compaction, cementation, sorting or clay content in a formation increases both R and V_p and decreases porosity. Trends in data on an $R/R_w - V_p$ plot differ because of changes in the pore space characteristics and/or the mineral constituents, which may or may not influence the pore space. Since electrical currents and acoustic waves are both influenced by similar pore space characteristics, location of data on an $R/R_w - V_p$ plot can be used to (1) identify changes in a formation's properties and (2) delineate individual formations with different characteristic properties. Because the R/R_w

– V_p bounds are so narrow, it could be difficult to distinguish different formation properties (Figure C6a); however, since the R/R_w – V_s bounds (Figure C6b) are wide, R/R_w – V_s data might provide more insight into the formation pore space characteristics.

Strictly speaking, the upper and lower bounds are defined for a specific fluid-mineral system. However, R/R_w and V_p values in a particular formation can vary from changes in the volumes of mineral constituents as well as changes in pore space characteristics. For example, in a quartz sand system, the HS and empirical upper bound is lower for a clay-cemented system than a quartz-cemented one since $R_{cl} < R_{qz}$, $V_{p\text{-}cl} < V_{p\text{-}qz}$ and $\phi_{c\text{-}cl} > \phi_{c\text{-}qz\text{-}sa}$. The influence of mineral constituents is particularly important to understand when interpreting the location of R/R_w – ϕ and V_p – ϕ data with respect to the bounds since the bounds themselves must be adjusted for changes in mineralogy.

By adding a cementing mineral with similar electrical and elastic properties as the granular constituent, the system's stiffness increases and porosity decreases resulting in increased in V_p and R. Such cemented data tend to plot near the empirical upper R/R_w –ϕ and V_p – ϕ bounds, therefore plot near the upper R/R_w – V_p bound (dotted line in Figure C6a).

The lower HS bounds on R/R_w and V_p characterize systems of resistive and stiff spheres in suspension, respectively, a likely model for many sediments. Consequently, data in clean sands and spheres fall on the lower HS R/R_w and V_p bounds when in suspension and just above when loosely packed. Therefore, data that plot near the lower HS bounds (bold dashed line in Figure C6a) are likely from unconsolidated and uncompacted sediments.

If the system's mineralogy doesn't change, decreasing the sorting (increasing the grain size distribution) decreases porosity and slightly increases the system's stiffness and tortuosity, leading to a slight increase in V_p and R. R/R_w – V_p data should plot up the lower HS bound as a result of decreased sorting. In many clastic depositional environments, however, sorting decreases from increasing clay content; the influence of sorting in such a case is the same as the clay influence.

The effects of clays on R and V_p are quite complex because of the unique electrical, elastic and pore space properties of clays. The influence of clays on the R and V_p of a system depends on the distribution of clays (dispersed, structural or cementing), the

method of adding the clays to the system (replacing pore space or grains), the properties of the other constituents (R_w, K_m and μ_m), and the compaction history. For example, consider the case where dispersed clays are added to the pore space of brine-saturated sand. In such a case, total porosity decreases because it is replaced by the clay volume. R increases because the channel porosity decreases and the tortuosity effect dominates over the conductivity effect. V_p also increases because the clays stiffen the pore space.

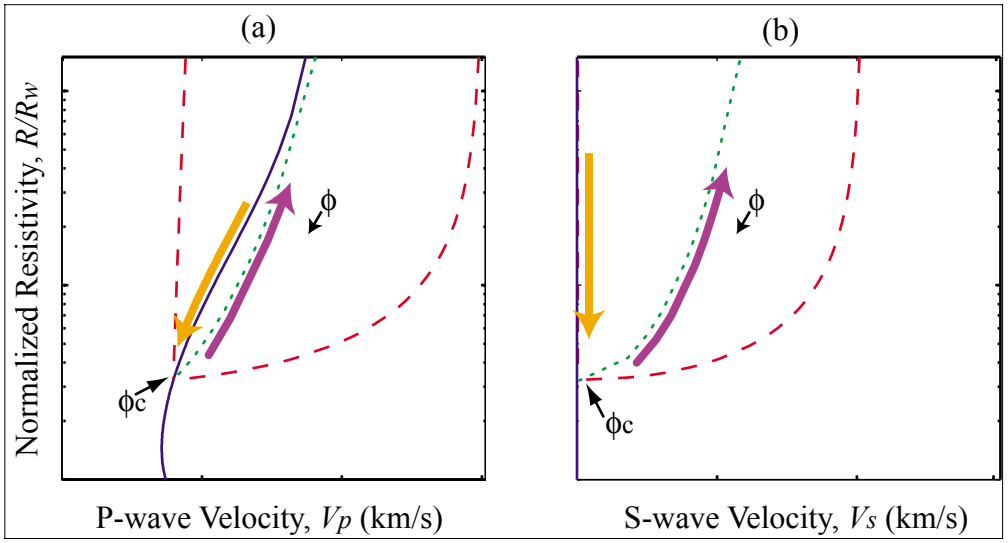

Figure C6: Using the velocity – resistivity bounds to evaluate formation properties. The arrows indicate the direction of increased change in pore space characteristic.

Conclusions

- For materials in suspension ($\phi > \phi_c$), the $R/R_w - V_p$ relationship is simply defined by the lower HS bounds on R and V_p.

- For grain-supported materials ($\phi < \phi_c$), the $R/R_w - V_p$ relationship is constrained by $R/R_w - V_p$ bounds, which are defined by the lower HS bounds for R and V_p and modified upper bounds for R/R_w and V_p.

- $R/R_w - V_p$ data in unconsolidated systems fall along the lower HS $R/R_w - V_p$ bound.

- $R/R_w - V_p$ data in cemented systems fall along the empirical upper $R/R_w - V_p$ bound.

- The $R/R_w - V_p$ bounds can be used to (1) constrain porosity estimates given $R/R_w - V_p$ data, (2) forward model $R/R_w - V_p$ data pairs given ϕ data.

- The trends of $R/R_w - V_s$ data with respect to the bounds may provide insight into changes in a formation's pore space characteristics.

References

Avseth, P., Mavko, G, Dvorkin, J., and Rykkje, Johannes, 1998. The effects of sorting on the rock physics properties of sands. *Stanford Rock Physics & Borehole Geophysics Project: Annual Report*, 68, Paper A3, 1-7.

Dvorkin, J., and Nur, A., 1996. Elasticity of high-porosity sandstones: Theory for two North Sea datasets. *Geophys*., 61, 1363-1370.

Han, D.H., 1986. *Effects of Porosity and Clay Content on Acoustic Properties of Sandstones and Unconsolidated Sediments*. Ph.D. dissertation, Stanford University.

Hashin, Z., and Shtrikman, S., 1963. A variational approach to the theory of the elastic behavior of multiphase materials. *J. Mech. Phys. Solids*, 11, 127-140.

Mavko, G., Mukerji, T., and Dvorkin, J., 1998, *The Rock Physics Handbook: tools for seismic analysis in porous media*, Cambrige University Press.

Mindlin, R.D., 1949. Compliance of elastic bodies in contact. *J. Appl. Mech.*, 16, 259-268.

Nur, A., Mavko, G., Dvorkin, J., and Gal, D., 1995. Critical Porosity: The key to relating physical properties to porosity in rocks, in *Proc., 65th Ann. Int. Meeting, Soc. Expl. Geophys*., 878.